AD_____

Award Number: DAMD17-00-1-0469

TITLE: Towards an Atomic Understanding of Double-Strand Break
Repair: Crystal Structure of Human RAD52 Protein

PRINCIPAL INVESTIGATOR: Wasantha K. Ranatunga
Gloria Borgstahl, Ph.D.

CONTRACTING ORGANIZATION: The University of Toledo
Toledo, Ohio 43606-3390

REPORT DATE: July 2002

TYPE OF REPORT: Annual Summary

PREPARED FOR: U.S. Army Medical Research and Materiel Command
Fort Detrick, Maryland 21702-5012

DISTRIBUTION STATEMENT: Approved for Public Release;
Distribution Unlimited

The views, opinions and/or findings contained in this report are
those of the author(s) and should not be construed as an official
Department of the Army position, policy or decision unless so
designated by other documentation.

20021127 127

REPORT DOCUMENTATION PAGE

Form Approved
OMB No. 074-0188

1. AGENCY USE ONLY (Leave blank)	2. REPORT DATE July 2002	3. REPORT TYPE AND DATES COVERED Annual Summary (15 Jun 01 – 14 Jun 02)

4. TITLE AND SUBTITLE
Towards an Atomic Understanding of Double-Strand Break Repair: Crystal Structure of Human RAD52 Protein

5. FUNDING NUMBERS
DAMD17-00-1-0469

6. AUTHOR(S)
Wasantha K. Ranatunga
Gloria Borgstahl, Ph.D.

7. PERFORMING ORGANIZATION NAME(S) AND ADDRESS(ES)

The University of Toledo
Toledo, Ohio 43606-3390

E-Mail: wranatunga@hotmail.com

8. PERFORMING ORGANIZATION REPORT NUMBER

9. SPONSORING / MONITORING AGENCY NAME(S) AND ADDRESS(ES)

U.S. Army Medical Research and Materiel Command
Fort Detrick, Maryland 21702-5012

10. SPONSORING / MONITORING AGENCY REPORT NUMBER

11. SUPPLEMENTARY NOTES

12a. DISTRIBUTION / AVAILABILITY STATEMENT
Approved for Public Release; Distribution Unlimited

12b. DISTRIBUTION CODE

13. Abstract *(Maximum 200 Words) (abstract should contain no proprietary or confidential information)*

Defects in recombination-based DNA repair lead to human breast cancer and familial degenerative diseases. The RAD52 epistasis gene products, especially the human RAD52 protein plays important role in double-strand break (DSB) repair. The focus of this work is to further understanding of the molecular basis of DSBs by solving the three-dimensional structure of hRAD52 and this will contribute a detailed understanding of the molecular mechanisms of breast cancer. The hRAD52 forms ring structure in solution and multiple level of aggregation of rings. We studied its multiple levels of self-association and stability using dynamic light scattering (DLS) and differential scanning calorimetry (DSC). To investigate the basis for the extreme stability of RAD52 that was discovered, two mutants were also studied, RAD52 (1-192) and RAD52 (218-418). We found that the aggregation is due to two levels of self-association of hRAD52, ring formation and association of rings with rings. DSC profiles and DLS data indicated that hRAD52 protein is extremely stable and multiple levels of self-association of hRAD52 can be disrupted by heating up to 50 °C. A hypothetical model of the effects of protein aggregation state on thermal stability was developed. Furthermore, a novel approach for purification of hRAD52 and for crystallization was established.

14. SUBJECT TERMS
DNA repair, x-ray crystallography, breast cancer

15. NUMBER OF PAGES
33

16. PRICE CODE

17. SECURITY CLASSIFICATION OF REPORT Unclassified	18. SECURITY CLASSIFICATION OF THIS PAGE Unclassified	19. SECURITY CLASSIFICATION OF ABSTRACT Unclassified	20. LIMITATION OF ABSTRACT Unlimited

Table of Contents

Manuscripts

Ranatunga, W., Jackson, D., Lloyd, J., Forget, A. L., Knight, K. L., and Borgstahl, G. E. O., Human RAD52 exhibits two modes of self-association. *J. Biol. Chem.,* **276**, 15876-15880 (2001).

Ranatunga, W., Jackson, D., Flowers II, R. A., and Borgstahl, G. E. O., Human RAD52 has extreme thermal stability. *Biochemistry*, **40**, 8557-8562 (2001).

Presentations

Wasantha Ranatunga, Human RAD52 has extreme thermal stability, The 22nd annual graduate research symposium, Sigma Xi Scientific Research society of The University of Toledo (April 20, 2001).

Wasantha Ranatunga, Doba Jackson, R. A. Flowers II and Gloria E. O. Borgstahl, Human RAD52 has extreme thermal stability. First Annual Biomolecular Sciences Day (March 24, 2001).

Gloria E. O. Borgstahl, Wasantha Ranatunga, Doba Jackson and Jeff Habel, Biochemical and structural studies on replication protein A and RAD52. Era of Hope: Department of defense Breast cancer research program meeting, proceedings vol. 1, p271 (2000).

Abbreviations

AT	ataxia telangiectasia
ATM	ataxia telangiectasia multifaceted
C_p	polydispersity
DLS	dynamic light scattering
DNA	deoxyribonucleic acid
DSB	double strand break
DSC	differential scanning calorimetry
EM	electron micrographs
HGP	hexylglucopyranoside
hRAD51	human RAD51 protein
hRAD52	human RAD52 protein
hRAD52(1+2)	human RAD52(1-192) protein
hRAD52(3+4)	human RAD52(218-418) protein
pBADhRAD52(wt)	wild-type thioredoxin fusion construct of human RAD52
R_H	hydrodynamic radius
RPA	replication protein A(human)
scRAD52	S. cerevisiae RAD52 protein
SOS	sum of squares (error)
T_M	melting temperature

Introduction

This is the second and final report for 3 year Pre-doctoral traineeship award (June 2000, DMAD17-00-1-0469) and following describes the progress made last 24 months.

This research project focuses on the study of human RAD52 (hRAD52) protein and the ultimate goal of our lab is to determine the crystal structure of hRAD52. The hRAD52 plays a central role in the repair of DNA double strand breaks (DSBs). Historically identified in yeast by its role in resistance to ionization radiation, hRAD52 has shown to be interacting with many proteins in the recombination based DSBs repair pathway.[1] Even though it is clear that RAD52 plays a crucial role in DSBs repair, the exact biochemical function of this protein has remained elusive. Recent findings indicate that two types of proteins are involved in DSBs repair: RAD52 and Ku. In lower eukaryotes (yeast), it is currently thought that DSBs are repaired by RAD52 dependent homologous recombination whereas in vertebrates repair is initiated by Ku dependent end joining.[2]

Once DSBs occur by ionizing radiation or chemical damage, RAD50/Mre11/Xrs2 protein complex process single stranded DNA (ssDNA) tails.[2] According to the recent model, hRAD52 or Ku binds these ssDNA tails. In particular, hRAD52 binding protects ssDNA ends from exonuclease digestion and stimulates ligation.[2] Two homologous recombination pathways have been proposed; ssDNA annealing can occur between repeated DNA sequences or stand invasion can occur after recruitment of hRAD51. Stand invasion involves the RAD52 epistasis group of proteins including replication protein A (RPA), RAD51, RAD52, RAD54, RAD55 and RAD57. RAD51 coats the ssDNA to form a filament with the assistance of RPA and searches for homologous sequence.[3] hRAD51 and RAD52 may act together at the ssDNA-binding step that proceeds homologous pairing.[4]

Recent findings indicated that there is direct link between DNA DSB pathway and breast cancer.[5] Germline mutations in the BRCA1 and BRCA2 genes are susceptible to breast cancer and ovarian cancer. About 52% of families of breast cancer cases found to be inherited with BRAC1 mutation and 32% of those to be inherited with BRCA2 mutation.[6,7] Furthermore, disruption of BRCA2 gene shows increased sensitivity to DNA damage caused by ionizing radiation. hRAD51 interacts with tumor-suppressor gene products, BRCA2 and BRCA1.[5,7] The association between BRCA2 and RAD51 was found to be direct using yeast-two hybrid assay and association between BRCA1 and RAD51 was thought to be through another protein.[5,7] This indicates BRCA2 may be an essential cofactor in the RAD51 dependent DNA DSB pathway. Studies on ataxia telangiectasia (AT), pleiotropic recessive disease indicated that RAD51 required interacting AT multifaceted gene product, ATM.[8] Particularly, mutation in AT gene has been linked to familial breast cancers.[9] AT is an autosomal recessive disorder with many phenotypic characteristics, including hypersensitivity to ionizing radiation and cancer predisposition.[10,11] The DSBs repair in AT cells found to be defective. Current findings show that assembly of RAD51 and RAD52 in recombination requires ATM and nonreceptor kinase c-Abl.[12]

hRAD52 interact with hRAD51 and RPA and is essential for DSB repair process.[13,14] hRAD52 also has self-associating region and has been shown to bind to DNA ends, promote end-to-end interactions and to form ring structures in electron

micrographs (Fig. 1).[15,16] Of particular interest to this research is that hRAD52 forms heterogeneous ring structures that vary in size from 10-30 nm diameter depending on the protein concentration.[15] Due to the formation of large aggregates in solution, hRAD52 is hard to work with for crystallization. Our main objective for solving this problem is to find conditions for disrupting large aggregates. In the first two years of this research, this objective was achieved and preliminary crystalline aggregates were obtained, as discussed below.
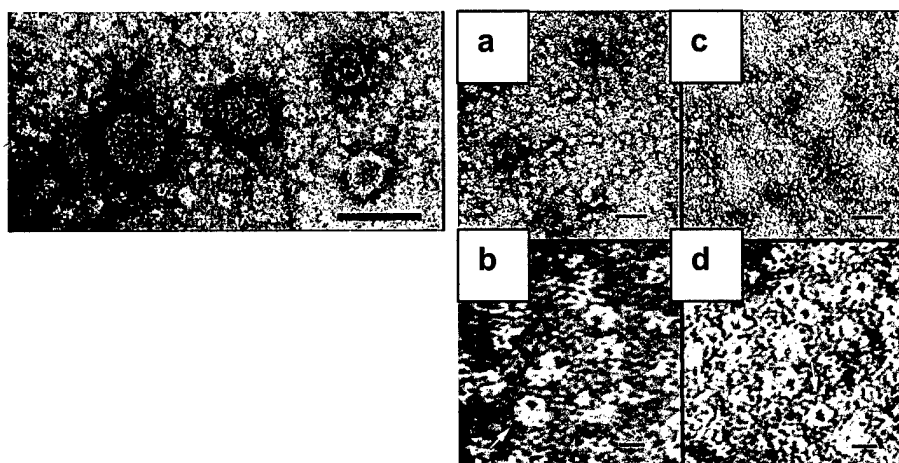

Figure 1 EM analysis of hRAD52 constructs

(A).Negative stained EM of hRAD52 protein
(B).Negative stained EM of hRAD52 and hRAD52(1-192) protein. Both hRAD52 (a and b) and hRAD52(1-192) (c and d) form 10 nm diameter ring shaped oligomers. Larger particles of hRAD52 in B are not formed by hRAD52(1-192) C(c, d). (adapted from Ranatunga et. al [17])

Body

Objective 1: Scale up of purification several forms of hRAD52

This objective was fulfilled for wild-type hRAD52 and hRAD52(1+2). hRAD52(3+4) purification was performed near homogeneity and scaled up by other member of our lab. The purification of pBADhRAD52(wt) and pBADhRAD52 (domain 1) were not pursued any further instead S. cerevisae RAD52 (scRAD52) and scRAD52(34-207) were purified for comparison with human counterparts. All the constructs (Fig. 2) were purified with large quantities and purified quantities were higher than reported. About 9.5 mg of hRAD52 and 8.0 mg of hRAD52(1-192) could be purified per gram of cell pellet (200 mL of
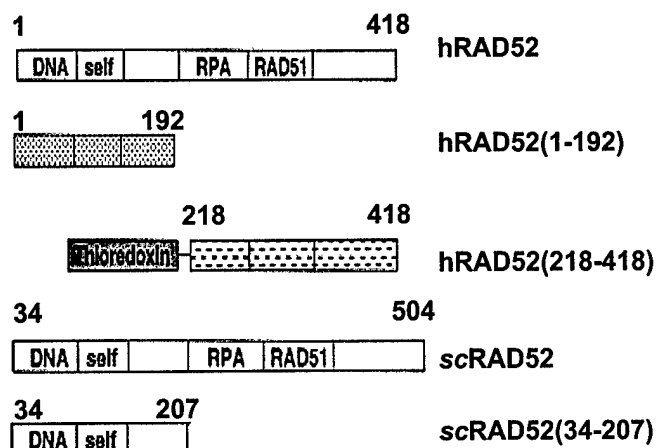
Figure 2 Schematic diagram of hRAD52, scRAD52 and their deletion mutants
Beginning and ending residue numbers of each mutant were indicated along with domain structure. hRAD52(1-192) is referred as hRAD52(1+2) and hRAD52(218-418) is referred as hRAD52(3+4) in the text. The domains and residue numbers are defined by park et. al: DNA binding, 39-80; self-association, 85-159; RPA binding, 221-280; RAD51 binding, 290-330.

cells). This was a much large quantity than reported in the literature. Benson et. al[13] have reported 3.2 mg per 4 L of E. coli FB810 pLysS cells. Van Dyck et. al have reported that 1.5 mg of protein was recovered from 5×10^{10} Sf9 insect cells.[16] About 1 mg of scRAD52 and 2-3 mg of scRAD52(34-207) per gram of cell pellet could be obtained and this amount was also higher than reported in the litrature.[15] Shinohara and Ogawa were reported 1-2 mg of scRAD52 per 10 g of E. coli 594 cells.[15]

Solution conditions of hRAD52 and hRAD52(1+2) were improved by including 2 mM HGP in the purification buffers after investigating several detergents and different pH conditions. Those conditions were monitored for monodisperse protein solution for crystallizability using DLS. hRAD52 found to be thermally stable and thus a heat step was included in the purification step. Purified with heat step, hRAD52 shows monomodal protein solution with closer to monodispersity ($Cp/R_H=39.7\%$) (Table 1). However, scRAD52 found to be aggregated in solution as similar to hRAD52. scRAD52 found to be monomodal in solution when purified with heat step.

With a collaboration of Dr. Kendall Knight at University of Massachusetts, we could be able to study aggregation state of hRAD52 and mutants of RAD52 using EM. EM studies confirmed our interpretation of DLS results (Table 1). As a summary, it appears that there are two levels of self-association for hRAD52, ring formation and association of rings with rings. The N-terminal half of the protein forms rings and C-terminal half is responsible for association between rings. These results were published in Journal of Biological Chemistry.[17]

The wild-type hRAD52 and hRAD52(1+2) forms rings with seven monomers in solution.[18] This study moves to find condition to dissociate large aggregates into monomers or smallest aggregates (rings) possible. We collected DSC data on wild-type

Table 1. DLS data for hRAD52: effect of HGP with concentration

Line #	DLS Experiment	Conc. (mg/mL)	Base -line	SOS error	R_H[a] (nm)	Peak Area[b] (%)	structural interpretation[c]
1	Concentrated to 3.5 mg/mL	3.5	1.004	0.58	6.1(0.8) 23.3(2.7) 1110(68.3)	6.4 90.0 3.6	1 ring >2 rings aggregates/ micelles
2	Concentrated to 3.5 mg/mL and added 2 mM HGP	3.5	1.009	5.63	10.1(1.0) 29.8(2.6)	23.9 76.1	1 ring >2 rings
3	Concentrated to 15 mg/mL and added 2 mM HGP	15.0	1.009	4.53	9.0(1.1) 27.6(3.2) 1100(6.8)	21.0 78.4 0.6	1 ring 2-3 rings aggregates/ micelles
4	hRAD52(1+2)	15.0	1.002	2.2	5.7(0.6) MW: 194(0.7) kD	100 Cp/R_H= 21.5%	1 ring

[a]Average R_H is given with the standard deviation given in parenthesis. [b]DynaLS results; DLS measurements at 20 and 50 °C on solvent alone indicate that very small and very large components in the hRAD52 measurements were due to solvent and not the protein. [c]Interpretation is based on estimated R_H.[19]
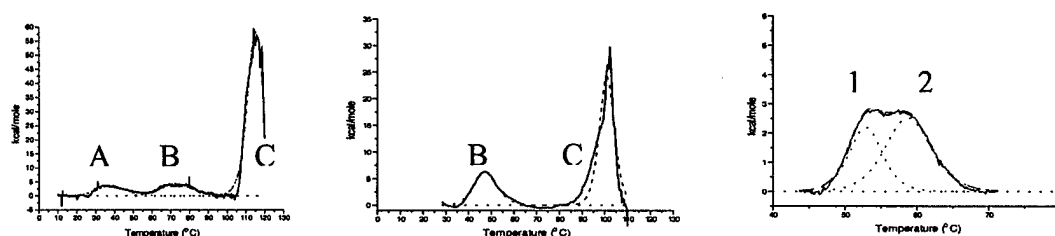
Figure 3. Thermal stability of hRAD52 and scRAD52 and mutants
Thermal stability profile was obtained from MicroCal DSC and analyzed using Origin™ software at (A) wild-type hRAD52 (0.038 mM, 3.5 mg/mL) (B) hRAD52(1+2) (0.325 mM, 7.2 mg/mL) (C) hRAD52(3+4) (0.082 Mm, 3.1 mg/mL)

Table 2 Thermodynamic parameters from DSC measurement of hRAD52 proteins

| protein	Concentration (mg/mL)	Component[¥]	T_M (°C)
hRAD52	3.5	A B C	38.8 73.1 115.2
hRAD52(1-192)	7.2	B C	47.6 100.9
hRAD52(218-418)	3.1	1 2	53.4 59.1

[¥]Components are indicated in Fig .3.

-contains unpublished data-

and mutant hRAD52 (Fig. 3, Table 2). Wild-type hRAD52 is extremely stable. The DSC data show three transitions for hRAD52 and two transitions for hRAD52(1+2). The first transition is probably due to the disruption of the super-ring complex, the second transition disruption of rings and third transition to total unfolding. This discovery has been very important. We have introduced a heat step in the purification of the protein and have achieved better purity than ever before. To support the observation of DSC data, we have used DLS at different temperatures and concentrations to study transitions (Table 3). Based on DLS and DSC data, a hypothetical four-state model for thermal denaturation of hRAD52 was proposed (Fig. 4). These results were published in Biochemistry Journal.[19] According to this study, the heat step can be used for the dissociation of large aggregates of hRAD52.
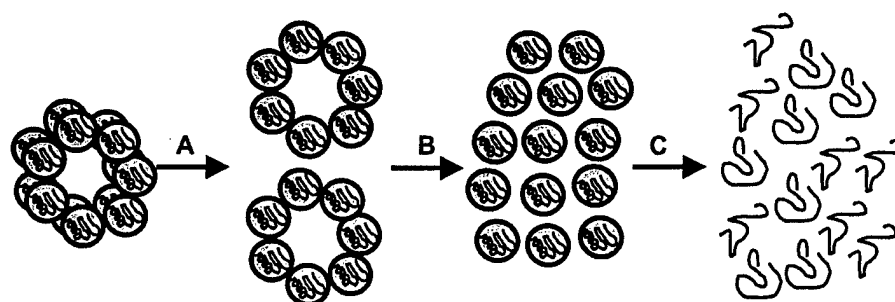
Figure 4 Hypothetical four-state modal for the thermal denaturation of wild-type hRAD52.

Transition A, B, and C corresponds to DSC Fig. 3. Transition A is attributed to disruption of higher order assemblies of hRAD52 rings, transition B to the disruption of rings to individual subunits, and transition C to complete unfolding. The individual subunits after transition B are probably partially unfolded as well as dissociated from the rings.

Similar studies were performed for purified scRAD52 and scRAD52(34-207). scRAD52 also forms ring-like structures observable by EM.[15] The scRAD52(34-207) mutant was designed by the Borgstahl lab to mimic hRAD52(1-192) and was not reported anywhere in the literature. EM pictures of the purified scRAD52 and scRAD52(34-207) show ring like structures and large aggregates for both scRAD52 and scRAD52(34-207) (Fig. 5). However, larger particles other than ring structures were not observed with hRAD52(1-192) in EM. Therefore, scRAD52(34-207) contains both types of self-association domains: formation of rings and higher order aggregates of rings. This was surprising because the self-association region and DNA binding regions of scRAD52 and hRAD52 share reasonable levels of homology.

-contains unpublished data-

Table 3 Effect of temperature and concentration on R_H of hRAD52

Line#	DLS Experiment	Conc. (mg/mL)	Base-line	SOS error	R_H[a] (nm)	Peak Area[b] (%)	Structural Interpretation[c]
1	20 °C	3.5	1.001	4.20	15.0(2.5)	98.3	>2 rings
2	heat to 50 °C for 30 min.	3.5	1.000	2.77	14.2(4.5)	99.2	~2 rings
3	concentrated, 20 °C	4.9	1.002	2.03	4.3 (0.5) 18.7(2.3)	3.4 95.8	monomer > 2 rings
4	concentrated, 20 °C	11.5	1.009	7.78	5.1(0.6) 17.8(3.1) 36.1(4.4)	4.2 56.9 36.6	mono/dimer >2 rings >>2 rings
5	heat to 50 °C, 30 min	11.5	1.000	5.96	19.2(8.5)	99.2	>2 rings
6	cool to 20 °C	11.5	1.010	8.24	5.9(0.4) 11.2(0.7) 20.6(2.2)	9.7 6.6 81.6	mono/dimer 1-2 rings >2 rings
7	11.5 mg/mL sample diluted to 3.5mg/mL, 20 °C	3.5	1.001	11.3	3.8(0.2) 23.2(11.6)	0.6 98.1	monomer >2 rings
8	heat to 50 °C, 30 min	3.5	1.001	9.41	9.7(1.2) 17.0(1.0)	45.8 49.8	1 ring >2 rings
9	cool to 20 °C	3.5	1.001	16.1	3.9(0.2) 11.9(1.9) 28.6(3.5)	1.1 69.3 26.4	monomer 1-2 rings >>2 rings
10	Sample from line 3 diluted; 20 °C	3.3	1.001	7.4	3.1(0.2) 16.8(5.4) 49.5(8.7)	11.0 84.0 14.5	Monomer >2 rings >>2 rings
11	Heat to 37 °C	3.3	1.000	7.9	19.8(10.9)	99.5	>2 rings
12	Sample from line 4 diluted; 20 °C	2.3	1.001	50.9	8.75(6.0)	79.7	1 ring
13	Heat to 37 °C	2.3	1.000	24.5	8.0 (1.6)	71.9	1 ring
14	Heat to 50 °C	2.3	1.000	15.9	8.7 (2.7)	87.4	1 ring

[a]Average R_H is given with the standard deviation given in parenthesis. [b]DynaLS results; the percent peak area for the solvent peaks was not reported. DLS measurements at 20 and 50 °C on solvent alone indicate that very small and very large components in the hRAD52 measurements were due to solvent and not the protein. Therefore, only the peaks attributable to hRAD52 protein are reported. [c]Interpretation is based on estimated R_H.[19]

DSC profiles show that scRAD52 was stable up to 60 °C at 0.5 mg/mL. However, increasing the concentration shifted the transition B and C to upper temperatures, which was similar to hRAD52 (Table 2 and 3). However, T_M of transition A was changed only 7 degrees from 0.5 to 2.5 mg/mL concentrations. It is important to note that scRAD52(34-207) seems more stable than scRAD52. scRAD52 is completely unfolded around 57-92

-contains unpublished data-

°C over the concentration range studied whereas scRAD52(34-207) unfolded around 84-99.3 °C. This suggests that C-terminal domain of scRAD52 has a destabilizing effect. This observation is opposite for hRAD52 protein in which the last two domains of hRAD52 increased the thermal stability.
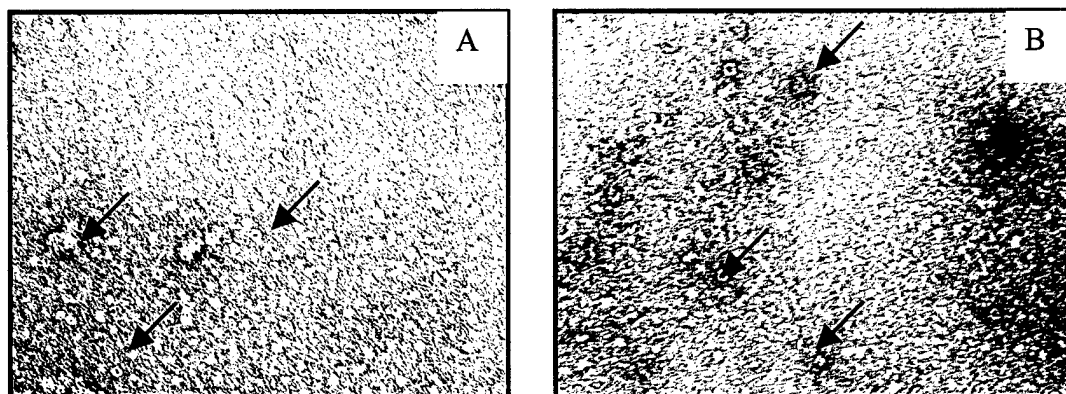
Figure 5 EM of scRAD52 proteins

(A) scRAD52 (B) scRAD52(34-207).
Arrows in black indicate ring-like structures in the micrographs. Arrows in blue indicate some higher order aggregates. Note that scRAD52 purification for this EM experiment contained a heat-step. Size of the ring in scRAD52 is 10 nm. In addition, 13 nm, 26 nm 52 nm particles/aggregates were visible. Size of the ring in scRAD52(34-207) is approximately 13 nm and aggregates in scRAD52(34-207) are about 26-34 nm.
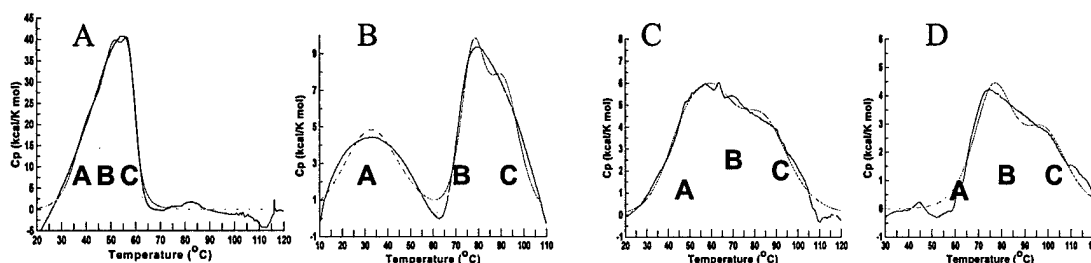
Figure 6 DSC profiles for scRAD52(34-207) and hRAD52 proteins.

DSC profile for scRAD52 for (A) 0.58, (B) 2.50, 1.64 mg/mL. DSC profile for RAD52(34-207) for (C) 0.69 and (D) 1.90 mg/mL.The curves were fit with minimized χ^2 values. Dashed red, solid red and solid blue lines represent fit curves, sum of curves and the data, respectively.

-contains unpublished data-

Table 4 Effect on concentration and temperature for *sc*RAD52 purified without heat step

Line #	DLS experiment	Conc. (mg/mL)	Base line	SOS error	R_H^a (nm)	Peak area[b]	Interpretation[c]
1	*sc*RAD52 @ 20 °C	0.66	2.017	14.8	13.9(1.4)	69.2	1-2 ring
2	*sc*RAD52 @ 20 °C	1.28	2.267	24.8	10.3(1.2)	57.6	1 ring
3	*sc*RAD52 @ 20 °C	1.96	2.542	40.2	8.8 (0.8)	57.3	1 ring
4	*sc*RAD52 @ 20 °C	3.7	2.226	20.1	8.7(0.9)	53.4	1 ring
5	*sc*RAD52 @ 20 °C	5.7	2.120	13.5	8.5(1.0)	53.6	1 ring
6	Heated to 30 °C	5.7	2.007	10.3	10.1(1.2)	55.3	1 ring
7	Heated to 37 °C	5.7	2.007	7.3	10.6(0.9)	52.6	1 ring
8	Heated to 45°C	5.7	2.004	5.6	10.8(1.2)	40.9	1 ring
9	Heated to 50 °C	5.7	2.017	3.6	10.4(1.3)	29.9	1 ring

[a, b, c] are similar to the footnote in Table 3.

DLS analysis confirmed that both *sc*RAD52 and *sc*RAD52(34-207) tended to aggregate upon concentration with different oligomeric states ranging from R_H of 6 to 30 nm with a reasonable percentage of massive aggregates. Similar to hRAD52, size of the diameter of *sc*RAD52 ring would be 9±1 nm.[15] In addition, aggregation level is high for *sc*RAD52(34-207) in comparison with hRAD52(1-192) (data not shown). With a similar argument, C-terminal part of *sc*RAD52 may have determinants for further aggregation of higher than two rings. Preliminary DLS experiments conducted for 0.5 to 5.77 mg/mL samples show that *sc*RAD52 tends to aggregate further on heating after 37 °C (Table 4). This indicates that the transition A of *sc*RAD52 in DSC attributable to some unfolding of the protein rather than simple disruption of RAD52 aggregates of rings.

The stability of *sc*RAD52(34-207) was higher than hRAD52(1-192) and *sc*RAD52 at similar concentrations (Table 5). The three transitions in the DSC profile are very close to each other. Unlike the human proteins, DLS data for *sc*RAD52(34-207) was similar to *sc*RAD52. Due to higher aggregate formation, *sc*RAD52 and *sc*RAD52(34-207) increased the thermal stability with concentration. This trend was also seen with hRAD52 but was diminished for hRAD52(1-192). Based on this information, *sc*RAD52 is relatively unstable compared to *sc*RAD52(34-207) and hRAD52. hRAD52 shows extreme stability over the range of temperatures. These results will be published in a journal and manuscript is in preparation.

-contains unpublished data-

Table: 3.5 DSC melting temperatures for scRAD52

Line #		Components*	Conc. (mg/mL)	T_M* (°C)	Conc. (mg/mL)	T_M (°C)
1	scRAD52	A	0.58	41.4	2.5	33.7
		B		51.8		77.9
		C		57.5		91.5
2	scRAD52 (34-207)	A	0.69	47.6	1.9	60.2
		B		62.0		77.1
		C		85.6		99.3

* Components are indicated in Fig. 6. Note, enthalpy values for each transition were not reported, because transitions were irreversible.

Objective 2 and 3: Crystal set ups (a) no DNA (b) with DNA and solve structures

The setting up crystal trays is already being achieved. As literature of crystallization implies, monodisperse protein solutions have better chance to have crystals over polydisperse solution. Most of the protein solutions of hRAD52, which were highly polydisperse or moderately polydisperse, did not crystallize. Monodisperse protein solution of hRAD52 with 3.5 mg/mL concentration produced some crystals with in a year, which seems to have crystalline shape. However, those crystals were very small. Increasing protein concentration or heating to 37°C or up to 50 °C before cooling down to 20 °C may help crystallization. Heating the sample improves the monodispersity due to separation of rings from aggregates and solubility of hRAD52 increases in the presence of crystallization regents. Trials are in progress. hRAD52(1-192) setups gave some promising birefringence, aggregates which were further screened with no reportable results. The setting up crystal trays with DNA was performed and showed some promising microcrystalline aggregates, which were too small to mount. In addition, setting up crystal trays of hRAD52 in the presence of RPA, a single strand DNA binding protein in DSB repair pathway, was set-up and showed similar microcrystalline aggregates. Those trials are in progress.

Since hRAD52 remained in solution and monodisperse at high temperature. An approach of crystallization at high temperature was considered. Since, two variables were working concurrently; vapor diffusion and evaporation due to heating, most of drops had evaporated and many produced salt crystals. Therefore, evaporation has to be slows down. For this purpose, crystallization under oil was investigated. Some oils like paraffin liquid slow down evaporation while heating. In addition, paraffin does not interact with the crystallization trials.[20,21,22] Microbatch trials were performed with a variety of conditions. However, it appeared that surface contacts and evaporation still generated salt crystals. To reduce the surface contacts, containerless crystallization was performed. Microbatch method has many advantages for producing large crystals, control of nucleation and control of surface contacts. However, most of drops were not placed in the middle of layer due to different composition and density of the drops. In addition, microbatch method with heating was not common or could not be found in the literature. Therefore, some drops sunk to bottom of the well, some were contacted with the surface

-contains unpublished data-

of the plate and produced salt crystals. To overcome this problem, sitting drop method with three depression spots was used and temperature was controlled using M6 incubators. At high temperature, proteins were in monodisperse condition and cooling down to 25 °C, and approached super saturation slowly. These trials are also in progress.

*sc*RAD52 found to be aggregated in solution and was less stable and heat step may not help for disrupting aggregates, as opposed to hRAD52. Even though *sc*RAD52 exist as monometer protein solution at °C and showed birefringent aggregates, crystallization of *sc*RAD52 at 50 °C may not be useful. Because DSC and DLS data indicated that *sc*RAD52 started unfolding upon heating. However, hRAD52 may withstand on heat up to 37 °C as DSC and DLS data implies. Therefore, hRAD52 may have better chance to crystallize at 37°C, rather than 50 °C.

Key Research Accomplishments

- Purification of hRAD52 proteins that are homogeneous and suitable for crystallization.
- EM and DLS data indicate that the N-terminal half of hRAD52 is involved in ring formation and C-terminal half is responsible for super ring aggregation (two modes of self-association).
- Scanning transmission electron microscopy (STEM) mass analysis and EM studies on hRAD52 proteins, performed in collaboration with Dr. Kendall Knight's group, confirmed the ring structure and super aggregation state of hRAD52.
- Differential scanning calorimetry (DSC) data indicates that hRAD52 has extreme thermal stability.
- Using DSC and DLS data, a four-state model for thermal denaturation of human RAD52 protein could be proposed.
- Based on DSC and DLS data, a novel approach for purification of hRAD52 and for crystallization was attempted.
- *sc*RAD52 constructs were purified to near homogeneity and DLS data were multimodal.
- DSC data indicates that *sc*RAD52 is less stable than hRAD52.
- Initial microcrystalline aggregates of hRAD52 and *sc*RAD52 were obtained

Reportable Outcomes

Manuscripts, abstracts, presentations (attached in appendix)

Manuscripts

Ranatunga, W., Jackson, D., Lloyd, J., Forget, A. L., Knight, K. L., and Borgstahl, G. E. O., Human RAD52 exhibits two modes of self-association. *J. Biol. Chem.,* **276**, 15876-15880 (2001).

Ranatunga, W., Jackson, D., Flowers II, R. A., and Borgstahl, G. E. O., Human RAD52 has extreme thermal stability. *Biochemistry,* **40**, 8557-8562 (2001).

Ranatunga, W., and Borgstahl, G. E. O., Manuscript on *sc*RAD52 is in preparation

Presentations

Wasantha Ranatunga, Human RAD52 has extreme thermal stability, The 22nd annual graduate research symposium, Sigma Xi Scientific Research society of The University of Toledo (April 20, 2001).

Wasantha Ranatunga, Doba Jackson, R. A. Flowers II and Gloria E. O. Borgstahl, Human RAD52 has extreme thermal stability. First Annual Biomolecular Sciences Day (March 24, 2001).

Gloria E. O. Borgstahl, Wasantha Ranatunga, Doba Jackson and Jeff Habel, Biochemical and structural studies on replication protein A and RAD52. Era of Hope: Department of defense Breast cancer research program meeting, proceedings vol. 1, p271 (2000).

Degree awarded

Doctor of Philosophy in Chemistry, August 2002.

Conclusions

Human RAD52 and hRAD52(1-192) and *sc*RAD52 proteins were purified near homogeneity with large quantity, which were suitable for crystallization based on DLS experiments. Initial experiments on DLS indicated that hRAD52 proteins and *sc*RAD52 proteins aggregated in solution due its inherent nature of self-association and formation of ring structure. Formation of aggregation is concentration dependant and disruption of these aggregates into monomeric molecule was a difficult task. The smallest size distribution with monodisperse protein solution found to be exists as a population of rings, with 8 nm hydrodynamic radius (2.3 mg/mL sample). However, the sample with 3.5 mg/mL concentration had better chance of crystallization. Most importantly, wild-type hRAD52 protein solution is monodispersed at 50 °C, even at 11.5 mg/mL and have

better chance for crystallization at 50 °C. hRAD52(1-192) protein solution was monodispersed at 15 mg/mL even at 20 °C, partly due to a lacking of C-terminal half, which would be a determining factor for aggregation. Unlike hRAD52, scRAD52 exists as monomodal protein solution at 5.7 mg/mL (Table 1). However, scRAD52(34-207) was not as monomodal as hRAD52(1-192). Most importantly, we could be able to produce hRAD52 protein solutions with monomodal condition, which was a difficult task, not reported in the literature.

We have found that hRAD52 has two modes of self-association based on EM, STEM and DLS studies. The N-terminal self-association domain mediates the assembly of monomers into rings, and previously unidentified domain in the C-terminal half of the protein mediates higher order self-association of rings. Scanning transmission electron microscopy, Size exclusion chromatography and DLS analysis indicate that hRA52(218-418) forms oligomeric particles containing 3-4 subunits and which would be player of higher aggregates.

Our data indicate that the RAD52 rings and higher ordered complexes of rings used in DNA repair and DNA recombination are extremely stable structures. The structure of wild-type RAD52 is very stable, and multiple levels of self-association appear to contribute to this stabilization. The extreme stability of the wild-type RAD52 and RAD52(1-192) folds relative to RAD52(218-418) appears to be related to the assembly of multiple monomers into a ring. The enhanced stability of wild-type RAD52 fold relative to hRAD52(1-192) appears to be due in part to its ability to form higher order assemblies of rings.

A four state hypothetical model has been developed to explain the thermal denaturation profile of wild-type RAD52 (Fig. 4). Individual rings of hRAD52 appear to have an R_H on the order of 8.0-8.75 nm in solution (Table 3, line 12-14). Higher order assemblies of rings are seen in the wild-type hRAD52 DLS data as particles ranging from 15-50 nm. Note that the measured R_H values are not integral values of individual rings due to presence of equilibrium mixtures of individual rings and complexes of rings in solution as indicated by high standard deviations in R_H measurements and width of DLS peaks. Raising the temperature from 20 to 50 °C disrupts the higher order particles, pushing the equilibrium toward the 9 nm particles. These data support our hypothetical model for transition A (Fig. 4). Reliable DLS measurements varying temperature on hRAD52(1-192) could not be made. Thermal expansion of the hRAD52(1-192) rings was noted.

Based on the stability of human and scRAD52 proteins, a novel approach on protein purification on hRAD52, that is heating the lysate to 50 °C, was developed. In addition, a novel approach on crystallization, by heating the crystallization set-ups to 50 °C, was developed. These discoveries made the protein crystallizable, one of the protein difficult to crystallize due to nature of aggregation. Preliminary crystalline aggregates of hRAD52, hRAD52(1-192) and scRAD52 were obtained.

References

[1] Shinohara, A., and Ogawa, T. Homologous recombination and the roles of double-strand breaks. *Trends in Biochem. Sci.*, **20**, 387-391 (1995).

[2] Van Dyck, E., Stasiak, A. Stasiak, A., and West, S. C., Binding of double-strand breaks in DNA by human RAD52 protein. *Nature,* **398**, 728-731 (1999).

[3] New, J. H., Sugiyama, T., Zaitseva, E., and Kowalczykowski, S. C., RAD52 protein stimulates DNA strand exchange by RAD51 and replication protein A. *Nature,* **391**, 407-410 (1998).

[4] Reddy, G., Golub, E. I., and Radding, C. M., Human RAD52 protein promotes single-strand DNA annealing followed by branch migration. *Mutat. Res.,* **377**, 53-59 (1997).

[5] Sharan, S. K., Morimatsu, M., Albrecht, U., Lim, D. -S., Regal, E., Dinh, C., Sands, A., Eichele, G., Hasty, P., and Bradley, A., Embryonic lethality and radiation hypersensitivity mediated by RAD51 in mice lacking BRAC2. *Nature,* **386**, 804-810 (1997).

[6] Ford, D., Easton, D.F., Stratton, M., Narod, S., Goldgar, D., Devilee,P., Bishop, D. T., Weber, B., Lenoir, G., Chang-Claude, Genetic heterogeneity and penetrance analysis of the BRCA1 and BRCA2 genes in breast cancer families. J. *Am. J. Hum. Gent.* **62**, 676-689 (1998).

[7] Wong, A. K. C., Pero, R., Ormonde, P., Tavtigian, S. V., and Bartel, P. L RAD51 interact with the evolutionary concerved BRC motifs in the human breast cancer susceptibility gene brca2. *J. Biol. Chem.* **272**, 31941-31944 (1997).

[8] Rotman, G. and Shiloh, Y. ATM: from gene to function *Hum. Molec.Genet.* **7**, 1555-1563 (1998).

[9] Jones, K., Brown, M. A., and Soloman, E. Molecular genetics of sporadic and familial breast cancer *Cancer surverys: Genetics and Cancer* **25**, 315-334 (1995).

[10] Swift, M. S., Reitnauer, P. J., Morrell, D., and Chase, C. Breast and other cancers in families with ataxia-telangiectasia. *The New Engl. J. Med.* **316**, 1289-1294 (1987).

[11] Swift, M. S., Morrell, D., Massey, R. B. and Chase, C. Incidence of cancer in 161 families affected by ataxia-telangiectasia. *The New Engl. J. Med.* **325**, 1831-1836 (1991).

[12] Chen, G., Yuan, S-S, F., Liu, W., Xu, Y., Trujillo, K., Song, B., Cong, F., Goff, S., Wu, Y., Arlinghaus, R., Baltimore, D., Gasser, P. J., Park, M. S., Sung, P., and Lee, E. Y. –H Radiation induced assembly of RAD51 and RAD52 recombination complex requires ATM and c-Abl. *J. Biol. Chem.,* **274**, 12748-12752 (1999).

[13] Benson, F. E., Baumann, P., and West, S. C. (1998) Synergistic actions of RAD51 and RAD52 in recombination and DNA repair. *Nature* **391**, 401-404 (1996).

[14] Park, M.S., Ludwig, D. L., Stigger, E., and Lee, S.-H. Physical interaction between human RAD52 and RPA is required for homologous recombination in mammalian cells. *J. Biol. Chem.* 271, 18996-19000.

[15] Van Dyck, E., Hajibagheri, N. M. A., Stasiak, A., and West, S.C. Visualisation of human RAD52 protein and its complexes with hRAD51 and DNA. *J. Mol. Biol.* **284**, 1027-1038 (1998).

[16] Shinohara, A., Shinohara, M., Ohta, T., Matsuda, S., and Ogawa, T. Rad52 forms ring structures and cooperates with RPA in single-strand DNA annealing. *Gene to cells* **3**, 145-156 (1998).

[17] Ranatunga, W., Jackson, D., Lloyd, J., Forget, A. L., Knight, K. L., and Borgstahl, G. E. O., Human RAD52 exhibits two modes of self-association. *J. Biol. Chem.,* **276**, 15876-15880 (2001).

[18] Stasiak, A. Z., Larquet, E., Stasiak, A., Muller, S. Engel, A., Dyck, E. V., West, S. C., and Egelman, E.H., The human RAD52 protein exists as a heptameric ring. *Curr. Biol.,* **10**, 337-340 (2000).

[19] Ranatunga, W., Jackson, D., Flowers II, R. A., and Borgstahl, G. E. O., Human RAD52 has extreme thermal stability. *Biochemistry*, **40**, 8557-8562 (2001).

[20] Chayen, N. Crystallization with oils: a new dimension in macromolecular crystal growth. *J. Cryst. Growth,* **196**, 434-441 (1999)

[21] D'Arcy, A., Elmore, C., Stihle, M., and Johnston, J. E. A novel approach to crystallizing proteins under oil. *J. Cryst. Growth*, **168**, 175-180 (1996)

[22] Chayen, N. The role of oil in macromolecular crystallization. *Structure,* **5**, 1269-1274 (1997)

Human RAD52 Exhibits Two Modes of Self-association*

Wasantha Ranatunga‡§, Doba Jackson‡§, Janice A. Lloyd§¶, Anthony L. Forget§¶, Kendall L. Knight¶, and Gloria E. O. Borgstahl‡∥

From the ‡Department of Chemistry, University of Toledo, Toledo, Ohio 43606-3390 and the ¶Department of Biochemistry and Molecular Pharmacology, University of Massachusetts Medical School, Worcester, Massachusetts 01655-0103

The human RAD52 protein plays an important role in the earliest stages of chromosomal double-strand break repair via the homologous recombination pathway. Individual subunits of RAD52 self-associate into rings that can then form higher order complexes. RAD52 binds to double-strand DNA ends, and recent studies suggest that the higher order self-association of the rings promotes DNA end-joining. Earlier studies defined the self-association domain of RAD52 to a unique region in the N-terminal half of the protein. Here we show that there are in fact two experimentally separable self-association domains in RAD52. The N-terminal self-association domain mediates the assembly of monomers into rings, and the previously unidentified domain in the C-terminal half of the protein mediates higher order self-association of the rings.

The repair of double-strand breaks in chromosomal DNA is of critical importance for the maintenance of genomic integrity. In *Saccharomyces cerevisiae*, genes of the *RAD52* epistasis group, *RAD50*, *RAD51*, *RAD52*, *RAD54*, *RAD55*, *RAD57*, *RAD59*, *MRE11*, and *XRS2*, were identified initially by the sensitivity of mutants to ionizing radiation (1, 2). These genes have been implicated in an array of recombination events including mitotic and meiotic recombination as well as double-strand break repair. *RAD52* mutants show the most severe pleiotropic defects suggesting a critical role for the protein in homologous recombination and double-strand break repair (2). The importance of specific protein-protein interactions in the catalysis of homologous recombination is suggested by studies demonstrating specific contacts and functional interactions between Rad52p and a number of proteins involved in recombination including Rad51p (3–8), which catalyzes homologous pairing and strand exchange, and replication factor A (RPA)[1] (8–10), a heterotrimeric single-stranded DNA binding protein (11).

Studies of the equivalent human proteins have identified similar interactions between the RAD52, RAD51, and replication protein A proteins (12–17). Based on a series of protein-protein interaction assays (15, 16, 18) and DNA binding studies[2] (16), a domain map of RAD52 was proposed by Park *et al.* (16) (see Fig. 1). The determinants of self-association were proposed to exist exclusively within a region defined by residues 65–165, a result supported by recent studies of several isoforms of RAD52 (19). Electron microscopy (EM) studies of Rad52p and RAD52 have revealed formation of ring-shaped structures (9–13 nm in diameter), as well as higher order aggregates (9, 12, 20). Stasiak *et al.* (21) performed image analyses of negatively stained electron micrographs and determined that the 10-nm RAD52 rings are composed of seven subunits. Scanning transmission electron microscopy (STEM) analysis indicated a mean mass of 330 ± 59 kDa supporting a heptameric ring-shaped RAD52 structure (21). Recent studies show that RAD52 binds to double-stranded DNA ends as an aggregated complex (20). These end-binding complexes were amorphous in shape and ranged in size from 15 to 60 nm. Within these complexes, RAD52 rings were observed occasionally. Binding of RAD52 to the DNA ends promoted end-to-end association between DNA molecules and stimulated ligation of both cohesive and blunt DNA ends (20).

Therefore, given that the formation of both ring-shaped oligomers and aggregates of these rings seem relevant to RAD52 function, we sought to investigate further the self-association properties of the RAD52 protein. We performed a series of analyses comparing full-length RAD52-(1–418) with two different mutant RAD52 proteins: (i) a 1–192 mutant that spans the N-terminal portion and includes the entire proposed DNA binding and self-association domains and (ii) a 218–418 mutant that spans the C-terminal portion of RAD52 that includes the proposed RPA- and RAD51-binding domains (Fig. 1). In contrast to previous studies, our results show that there are experimentally separable determinants for two different modes of self-association by RAD52, one in the N-terminal and one in the C-terminal portion of the protein.

EXPERIMENTAL PROCEDURES

RAD52 Constructs—Wild-type *RAD52* and *RAD52*-(1–192) pET28 expression plasmids were a gift from Dr. M. Park and have six histidines fused to the C terminus. A pET28 expression plasmid containing the thioredoxin-RAD52-(218–418) fusion protein was constructed using standard polymerase chain reaction techniques.

Protein Purification—Cultures of transformed BL21(DE3) Codon Plus *Escherichia coli* (Stratagene) were grown in a fermentor and induced with 0.5 mM isopropyl-1-thio-β-D-galactopyranoside. Wild-type *RAD52* and *RAD52*-(1–192) cells were resuspended in a buffer consisting of 20 mM HEPES, pH 6.0, 10% glycerol, 400 mM NaCl, 100 mM KCl, 5 mM β-mercaptoethanol, 1 mM dithiothreitol, 1 mM hexylglucopyranoside, and 1 mM EDTA. *RAD52*-(218–418) cells were resuspended in a

§ These authors contributed equally to this work.

∥ To whom correspondence should be addressed: Dept. of Chemistry, University of Toledo, 2801 W. Bancroft St., Toledo, OH 43606-3390. Tel.: 419-530-1501; Fax: 419-530-4033; E-mail: gborgst@uoft02.utoledo.edu.

[1] The abbreviations used are: RPA, replication protein A; MES, 4-morpholineethanesulfonic acid; EM, electron microscopy; STEM, scanning transmission electron microscopy; BSA, bovine serum albumin; DLS, dynamic light scattering.

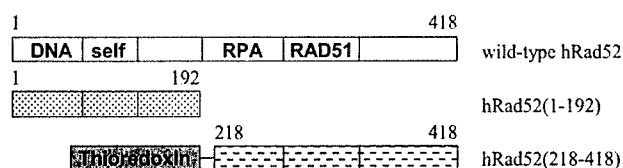[2] J. A. Lloyd, and K. L. Knight, unpublished data.

FIG. 1. **Schematic diagram of wild-type RAD52 and deletion mutants.** The beginning and ending residue numbers of each mutant are indicated along with domain structure. The following domains and residue numbers were defined by Park *et al.* (16): DNA binding, 39–80; self-association, 85–159; RPA binding, 221–280; RAD51 binding, 290–330.

buffer consisting of 50 mM HEPES, pH 8, 500 mM KCl, 500 mM LiSO$_4$, 2.5% glycerol, 1 mM EDTA, 5 mM dithiothreitol, 4 mM imidazole, and 0.1% Triton X-100. Protease inhibitors (1 mM phenylmethylsulfonyl fluoride and 10 mM benzamidine) were used throughout purification. Cells were lysed using a French press, and the lysate was clarified by centrifugation, filtration through Cell Debris Remover-modified cellulose (Whatman), and passage through a 0.22-μm pore filter. The clarified lysate was applied to an MC/M Ni^{2+} affinity column (PerSeptive Biosystems) that was optimally washed and eluted with an imidazole gradient. Wild-type RAD52 and RAD52-(1–192) then were dialyzed extensively against a buffer consisting of 20 mM MES, pH 6.0, 10% glycerol, 400 mM NaCl, 100 mM KCl, 5 mM β-mercaptoethanol, 1 mM dithiothreitol, 1 mM hexylglucopyranoside, and 1 mM EDTA. RAD52-(218–418) was dialyzed extensively against a buffer consisting of 50 mM HEPES, pH 8.0, 2.5% glycerol, 2.5 mM EDTA, and 0.5 mM hexylglucopyranoside and then purified further by anion exchange using an HQ/M column (PerSeptive Biosystems) eluted with a KCl gradient. Protein samples were concentrated using Amicon concentrators with YM10 membranes, and protein concentrations were determined using Bradford assay (Bio-Rad) with bovine serum albumin (BSA) as a standard. The expression plasmid for wild-type RPA heterotrimer was a gift from Dr. M. Wold. RPA was expressed and purified as described (22).

Enzyme-linked Immunosorbent Assay—The enzyme-linked immunosorbent assay was done at room temperature. Briefly, 10 pmol of wild-type RAD52, RAD52 mutants, or BSA were coated to microtiter plates for 1 h. Plates were washed three times with phosphate-buffered saline (PBS) containing 0.02% Tween 20 to remove unbound protein. Plates then were blocked with 5% milk in PBS for 10 min and then washed. Various amounts of RPA in PBS and 5% milk were added and incubated for 1 h. Plates then were washed to remove nonspecific interactions and probed with a monoclonal antibody against the 70-kDa subunit of RPA (Calbiochem) in PBS and 5% milk for 30 min. Plates then were washed and probed with anti-mouse IgG peroxidase conjugate (Sigma) in PBS and 5% milk for 30 min and washed. Plates were developed using 3,3',5,5'-tetramethylbenzidine in phosphate-citrate buffer with 0.03% hydrogen peroxide. Color was developed for 30 min, the reaction was stopped with 1.5 M H$_2$SO$_4$, and absorbance readings at 450 nm were taken with a microtiter plate reader. Background absorbance was determined from a blank well and then subtracted from the data.

Gel-shift DNA Binding Assays—Reactions (20 μl) contained 20 mM triethanolamine-HCl, pH 7.5, 1 mM dithiothreitol, 1 mM MgCl$_2$, 0.1 mg/ml BSA, 0.05% Tween 20, 2 nM 5'-end-labeled 95 base oligonucleotide (concentration in bases), and the indicated amounts of protein. The oligonucleotide sequence is as follows: 5'-AGA CGA TAG CGA AGG CGT AGC AGA AAC TAA CGA AGA TTT TGG CGG TGG TCT GAA CGA CAT CTT TGA GGC GCA GAA AAT CGA GTG GCA CTA ATA AG-3'. Reactions were incubated at 37 °C for 20 min followed by the addition of glutaraldehyde to 0.2% and continued incubation at 22 °C for 20 min. Glycerol was added to a final concentration of 1.6% (w/v) and samples (10 μl) were loaded onto a 0.8% agarose gel and electrophoresed at 100 mV in 0.5× TBE buffer (90 mM Tris, 64.6 mM boric acid, and 2.5 mM EDTA, pH 8.3). Gels were analyzed using a Molecular Imager FX and QuantityOne software (Bio-Rad). The 95-base oligonucleotide used in the gel-shift assays was made using an ABI 392 DNA/RNA synthesizer.

Dynamic Light-scattering (DLS) Analysis—DLS was carried out using a DynaPro-801 molecular sizing instrument equipped with a microsampler (Protein Solutions). A 50-μl sample was passed through a filtering assembly into a 12-μl chamber quartz cuvette. For RAD52-(1–192) and RAD52-(218–418), 20-nm filters were used. For wild-type RAD52, a 100-nm filter was used. The data were analyzed first using Dynamics 4.0 software and then DynaLS software as follows. Hydrodynamic radii (R_H) for monomodal distributions, as defined by a baseline ranging from 0.977 to 1.002, were reported from Dynamics 4.0. Bi- and multimodal distributions were analyzed using DynaLS. DynaLS data estimates of molecular weight were obtained from R_H using Dy-
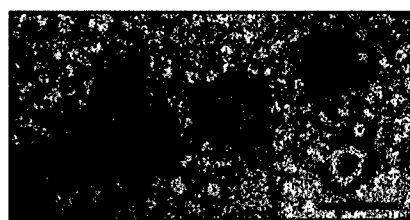

FIG. 2. **Negative stained electron micrograph of wild-type RAD52.** Wild-type RAD52 (4.0 μM) was prepared as described under "Experimental Procedures." Larger spherical particles are ~80 nm in diameter, half-spheres are 50 nm, and numerous 10-nm rings are visible also. *Black bar* = 0.1 μm.
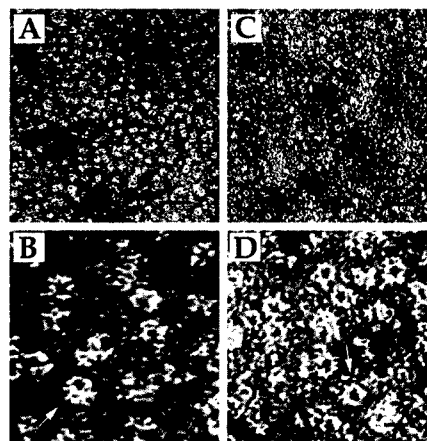

FIG. 3. **Negative stained electron micrographs of wild-type RAD52 and RAD52-(1–192) protein.** Proteins (4.0 μM) were prepared as described under "Experimental Procedures." The majority of protein for both wild-type RAD52 (*A* and *B*) and RAD52-(1–192) (*C* and *D*) forms 10-nm diameter ring-shaped oligomers. Larger particles of wild-type RAD52 in *A* (also see Fig. 2) are not formed by RAD52-(1–192). Higher magnifications of both proteins reveal that the protrusions observed on the 10-nm rings of wild-type RAD52 are missing in the RAD52-(1–192) rings (*arrows* in *B* and *D*). *Black bars* = 0.05 μm in *A* and *C* and 0.01 μm in *B* and *D*.

namics 3.0 molecular weight calculator. Sum of squares errors less than 5000 were considered negligible.

Electron Microscopy—Proteins were prepared for EM by diluting wild-type or mutant RAD52 to 4.0 μM in a buffer containing 20 mM Tris-HCl, pH 7.5, 5% glycerol, 5 mM β-mercaptoethanol, 0.1 mM EDTA, and 100 mM KCl. Samples were spread onto thin carbon films on holey carbon grids (400 mesh), stained with 1% uranyl acetate, and visualized by transmission electron microscopy using a Philips CM10 microscope.

STEM Analysis—Analyses were carried out at the Brookhaven National Laboratory using unstained, unshadowed freeze-dried samples. Protein samples (~0.1 mg/ml) were applied to a thin carbon film supported by a thick holey film on titanium grids and freeze-dried overnight. The microscope operates at 40 kV. Operation of the STEM and data analyses were performed as described previously (23).

Gel Filtration—Samples of the RAD52-(218–418) protein at 1.2 mg/ml were loaded onto a Superdex 200 HR 10/30 gel filtration column (Amersham Pharmacia Biotech/LKB) equilibrated in buffer containing 20 mM MES, pH 6.0, 400 mM NaCl, 100 mM KCl, 10% (w/v) glycerol, 5 mM β-mercaptoethanol, and 1 mM EDTA. Analysis was performed using a BioLogic chromatography system (Bio-Rad) with an in-line UV detector.

RESULTS

Oligomeric Characteristics of RAD52 Proteins—EM analyses of wild-type RAD52 and RAD52-(1–192) show that both proteins form ring-shaped structures (Figs. 2 and 3). The average diameter of these particles, measured across the surface with the central pore, is 10 ± 1 nm, consistent with previous reports (9, 12, 21). Wild-type RAD52 also forms distinct larger particles that appear as various sized spheres and half-spheres ranging in diameter from 30 to 100 nm (Fig. 2). These particles consist of individual 10-nm rings as well as other less distinct com-

FIG. 4. **STEM histograms.** STEM mass analyses were performed as described under "Experimental Procedures." Histograms include pooled data from several separate analyses (eight for wild-type RAD52, six for RAD52-(1–192), and five for RAD52-(218–418)). Average mass values were as follows: *A*, wild-type RAD52 298 ± 69 kDa (*n* = 309); *B*, RAD52-(1–192) 227 ± 30 kDa (*n* = 277); *C*, RAD52-(218–418) 153 ± 40 kDa (*n* = 119).

wild-type hRad52   **hRad52(1-192)**   **hRad52(218-418)**
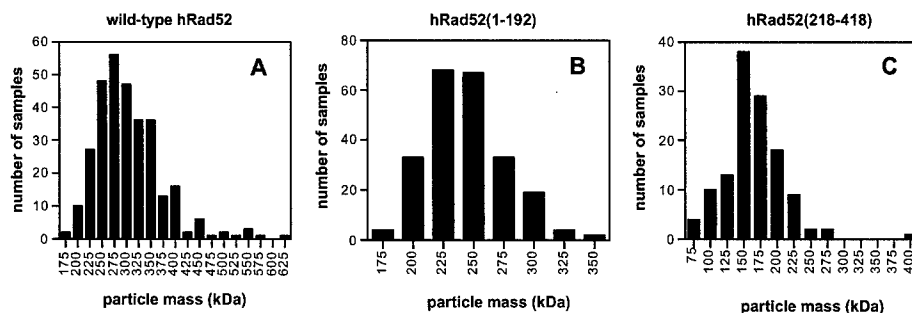
TABLE I

Dynamic light-scattering measurements of RAD52 proteins

Protein	Concentration	Base line	Modality	SOS[a]	$R_H{}^b$	Molecular mass	Peak[c] area
	mg/ml			*error*	*nm*	*kDa*	*%*
RAD52	3.5	1.007	Multimodal	3.10	6.6 (0.7)	279	10.5
					27.6 (9.3)	9.05×10^3	85.8
					711.0 (245)	2.40×10^7	3.7
RAD52-(1–192)	15	1.001	Monomodal	1.95	5.7 (1.2)	200	
RAD52-(218–418)	2	1.001	Monomodal	0.64	4.6 (2.1)	118	
Thioredoxin	1	1.001	Monomodal	3.3	2.0 (0.8)	14.8	

[a] SOS, sum of squares.

[b] Average hydrodynamic radius (R_H) is reported with the polydispersity (width of the distribution in nm) given in parentheses.

[c] For DynaLS results the percent peak area for the solvent peak is not reported.

pressed structures. For RAD52-(1–192) the majority of protein forms ring-shaped oligomers, and no larger particles were seen (Fig. 3). Even at increased concentrations (6 and 10 μM) RAD52-(1–192) shows no larger aggregates (data not shown). Higher magnifications reveal "protrusions" extending from the 10-nm rings formed by wild-type RAD52 that are missing in the 1–192 protein (see *arrows* in Fig. 3, *B* and *D*). These protrusions likely correspond to those modeled by Stasiak *et al.* (21), and our data show that they are part of the C-terminal portion of RAD52.

STEM analyses of wild-type RAD52 (2 μM) showed particle sizes ranging from 175 to 625 kDa with a mass average of 298 ± 69 kDa (*n* = 309; Fig. 4*A*). Given a molecular mass of 48 kDa for the His-tagged RAD52 protein, this range corresponds to particles that contain from 4 to 13 subunits with an average of six subunits. Similar analyses of the 1–192 protein showed particle sizes ranging from 100 to 350 kDa with a mass average of 227 ± 30 kDa (*n* = 277; Fig. 4*B*). For a monomer molecular mass of 23 kDa, this range corresponds to particles that contain from 4 to 15 subunits with an average of 10 subunits. Resolution of the ring-shaped oligomers in the electron micrographs was not high enough to count individual subunits, but our STEM data are consistent with previous work in which oligomeric rings of wild-type RAD52 were determined to be heptameric (21).

The oligomeric distribution of these proteins in solution was investigated by DLS. Wild-type RAD52 shows a multimodal profile with three peaks corresponding to particles with an average hydrodynamic radius of 6.6, 27.6, and 711.0 nm, respectively (Table I). These likely correspond to ring-shaped oligomers, the 30-nm particles described previously as "super-rings" (12) and seen in our micrographs (Fig. 2), and larger aggregates also observed in our micrographs. We find that the percent distribution of these various sized particles is effected by protein concentration, *i.e.* with increasing concentration the larger aggregates account for a larger percentage of the population. In contrast to wild type, RAD52-(1–192) shows a monomodal light-scattering profile that corresponds to a particle with a hydrodynamic radius of 6.1 nm (Table I), which is in agreement with our EM analysis.

The above analyses indicate at least two modes of RAD52 self-association that are experimentally separable, (i) forma-

hRad52(218-418)
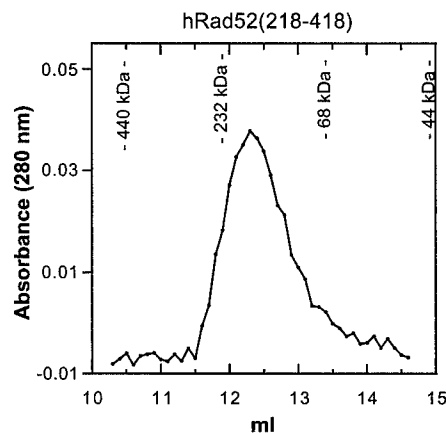
FIG. 5. **Gel filtration profile of the thioredoxin/218–418 fusion RAD52 protein.** The mutant protein (1.2 mg/ml, 35.8 μM) was loaded onto a Superdex 200 HR 10/30 gel filtration column, and elution of protein was followed at $A_{280 \text{ nm}}$. The indicated elution volumes of standards (ferritin, *440 kDa*; catalase, *232 kDa*; BSA, *68 kDa*; ovalbumin, *44 kDa*) were an average of four runs.

tion of ring-shaped oligomers and (ii) formation of larger aggregates. Because the latter seems to depend largely on the presence of residues C-terminal to position 192, we performed a number of assays to test for self-association on a mutant RAD52 containing only residues 218–418. Initial EM studies showed no distinct structural characteristics for this protein (data not shown), but STEM analysis revealed particle sizes ranging from 75 to 275 kDa (Fig. 4*C*) with a mass average of 153 ± 40 kDa (*n* = 119; Fig. 4*C*). Given a monomer molecular mass of 39 kDa, the particle composition ranges from two to seven subunits with an average of four subunits. Gel filtration shows a homogeneous peak corresponding to a molecular mass of 166 kDa (Fig. 5) and therefore to a particle containing approximately four subunits. Analysis by DLS shows a monomodal peak corresponding to a particle with an average R_H of 4.6 nm and a molecular mass of 118 kDa (therefore containing approximately three subunits). DLS measurements on thioredoxin alone show that it does not contribute to the oligomeric character of thioredoxin-RAD52-(218–418) (Table I). Together,

wt hRad52

hRad52(1–192)

nM | 0 5 10 20 40 60 80 100 250 500

nM | 0 5 10 20 40 60 80 100 250 500

FIG. 6. **Gel-shift DNA Binding assays.** Indicated concentrations of either wild-type RAD52 or RAD52-(1–192) were incubated with a 5′-end-labeled 95-base oligonucleotide followed by cross-linking with glutaraldehyde as described under "Experimental Procedures." Reactions were electrophoresed on a 0.8% agarose gel. Radioactive material at the *top* of the gel represents protein-DNA complex trapped in the gel well. *u*, unbound DNA; *b*, protein-DNA complex.
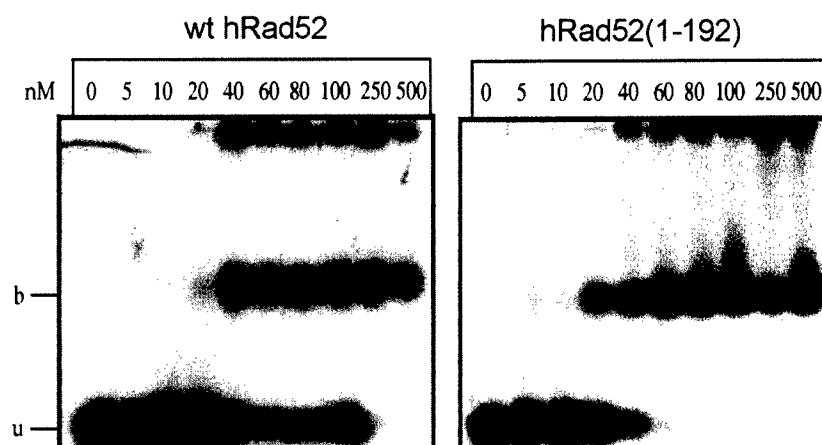
these data indicate that the C-terminal portion of RAD52 (residues 218–418) contains determinants of protein self-association that are distinct from those required to form 10-nm rings.

DNA Binding—Binding of wild-type RAD52 and RAD52-(1–192) to single-stranded DNA was analyzed by gel-shift assays. The gels in Fig. 6 are representative of five different experiments, each of which gave similar results. In each case, analysis of unbound and bound DNA (including that in the gel well) gave rise to a $K_{D(app)}$ of 35 and 25 nM for wild-type RAD52 and RAD52-(1–192), respectively. This slight enhancement in binding affinity was observed consistently for RAD52-(1–192). With wild-type RAD52 a significant portion of bound DNA remained in the gel well, a result that likely reflects the ability of the wild-type protein to form greater amounts of self-aggregates than the 1–192 mutant protein (see below). Additionally, 100% of the DNA (2 nM total nucleotides) was bound by the 1–192 protein at 40–60 nM protein in the titration profile, whereas 100% binding by wild-type RAD52 consistently required greater than 100 nM protein. Assays using the RAD52-(218–418) mutant protein showed no DNA binding up to 2.0 μM protein (data not shown). These results show that the DNA binding domain of RAD52 is contained within the N-terminal portion of the protein and that removal of the C-terminal 227 residues results in a slight enhancement of DNA binding.

Interaction of RAD52 Proteins with RPA—Previous studies have mapped residues 221–280 as the domain in RAD52 that interacts with the 32-kDa subunit of RPA (16). To ensure that the 218–418 mutant construct maintained a native fold, we tested this protein for interaction with RPA using an immunoassay. Enzyme-linked immunosorbent assays showed that the 218–418 protein interacted with RPA with an affinity similar to that observed for wild-type RAD52 (Fig. 7). No interaction with RPA was observed for RAD52-(1–192), thioredoxin, or BSA.

DISCUSSION

Previous studies have shown that RAD52 exists in a number of oligomeric states ranging from rings with a 10-nm diameter to larger complexes with diameters of greater than 30 nm (9, 12, 20, 21). Recent observations indicate a direct role for these higher order protein-protein interactions in promoting DNA end-joining (20). We therefore sought to investigate the self-association properties of RAD52 utilizing an array of biophysical techniques.

In our EM studies of wild-type RAD52 and RAD52-(1–192), we observed ring structures with an average diameter of 10 ± 1 nm as has been reported previously (9, 12, 20, 21). Additionally, and as seen previously (12, 20, 21), we observed protrusions extending from wild-type RAD52 rings as well as a population of distinct larger particles. However, neither the protrusions nor the larger particles were observed with RAD52-(1–192). This suggests that
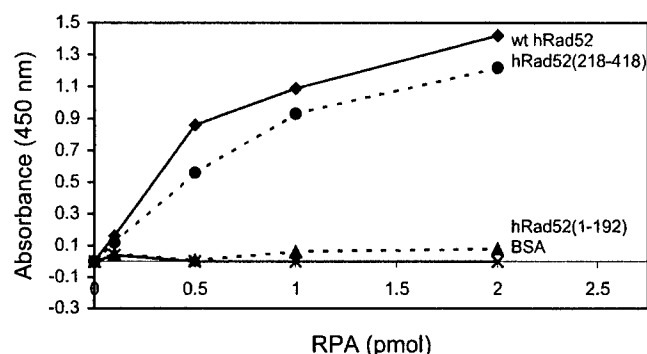
FIG. 7. **RAD52-RPA protein-protein interactions.** Enzyme-linked immunosorbent assays were performed as described under "Experimental Procedures" with RAD52 proteins immobilized to microtiter plates and probed with increasing amounts of RPA heterotrimer. The experiment was performed in triplicate, and the average for each RPA concentration was plotted. The error was on the order of 5–10%. *wt*, wild type.

residues within the C-terminal portion of the protein (residues 193–418) make up these protrusions and carry determinants for higher order RAD52 self-association.

DLS analysis of wild-type RAD52 and the two mutant proteins provides additional and complementary evidence for two distinct modes of RAD52 self-association. DLS analysis of wild-type RAD52 shows three peaks that likely correspond to the 10-nm ring-shaped oligomers and the 30-nm and larger particles observed by EM. In contrast, both RAD52-(1–192) and RAD52-(218–418) show a monomodal DLS profile indicating the presence of a single population of structures. The RAD52-(1–192) R_H is consistent with a ring structure, and the RAD52-(218–418) R_H indicates a complex composed of three subunits. This self-association of RAD52-(218–418) was confirmed by size-exclusion chromatography and STEM.

The ability of RAD52-(218–418) to self-associate was unexpected. Previous studies have suggested that residues 65–165 define the exclusive self-association domain in the RAD52 protein (18). Shen *et al.* (18) found that although N-terminal fragments of the protein self-associated in two-hybrid screens and affinity chromatography assays, fragments containing various portions of the C terminus, *e.g.* 287–418 or 166–418, did not. In contrast to these results, we find that RAD52-(218–418) is able to self-associate. Although our EM analysis revealed no distinct oligomeric structures for RAD52-(218–418), three different methods (STEM, gel filtration, and DLS) showed that this mutant formed oligomeric particles containing 3–4 subunits. These data for RAD52-(218–418), coupled with the inability of RAD52-(1–192) to form structures larger than the 10-nm rings, indicate that residues within the C-terminal region of the pro-

tein make important contributions to RAD52 self-association. Thus, the C-terminal region of RAD52 contains a novel self-association domain distinct from that previously identified within residues 65–165 (18).

Importantly, functional analyses of both the 1–192 and 218–418 mutant proteins show that each maintains an expected activity. Both wild-type RAD52 and the 1–192 proteins, which form ring-shaped oligomers, bound single-stranded DNA with similar affinities. This is consistent with previous studies that mapped the DNA binding domain of RAD52 to residues 39–80^2 (16). The elevated affinity of RAD52-(1–192) for single-stranded DNA was noted also for a similar Rad52p construct (24). Also as expected, RAD52-(218–418) showed a specific interaction with RPA. Again, this is consistent with previous studies that mapped the RPA interaction domain to residues 221–280 in RAD52 (16). The fact that both mutant proteins showed the expected functions demonstrates that they very likely maintain native structure, thereby supporting the relevance of differences observed in their oligomeric characteristics compared with wild-type RAD52.

In summary, our data support a model in which the self-association domain within the N-terminal region of RAD52 (residues 1–192) promotes the formation of ring-shaped oligomers that are functional for DNA binding, whereas the C-terminal domain (residues 218–418) mediates higher order self-association events. Additionally, the protrusions extending from the 10-nm ring structure of wild-type RAD52, originally modeled by Stasiak *et al.* (21) and seen clearly in our electron micrographs, correspond to the C-terminal region of the protein. Given the likely importance of higher order self-association to the ability of RAD52 to promote end-to-end joining of DNA breaks (20), these protrusions seem to mediate a critically important aspect of RAD52 function. Further studies of various mutant RAD52 proteins will clarify the contribution made by the different aspects of self-association toward the overall function of this important DNA repair protein.

REFERENCES

1. Game, J., and Mortimer, R. K. (1974) *Mutat. Res.* **24,** 281–292
2. Petes, T. D., Malone, R. E., and Symington, L. S. (1991) in *The Molecular and Cellular Biology of the Yeast, Saccharomyces* (Broach, J. R., Pringle, J. R., and Jones, E. W., eds) pp. 407–522, Cold Spring Harbor Laboratory Press, Cold Spring Harbor, NY
3. Shinohara, A., and Ogawa, T. (1998) *Nature* **391,** 404–407
4. Milne, G. T., and Weaver, D. T. (1993) *Genes Dev.* **7,** 1755–1765
5. Hays, S. L., Firmenich, A. A., and Berg, P. (1995) *Proc. Natl. Acad. Sci., U. S. A.* **92,** 6925–6929
6. Johnson, R. D., and Symington, L. S. (1995) *Mol. Cell. Biol.* **15,** 4843–4850
7. Sung, P. (1997) *J. Biol. Chem.* **272,** 28194–28197
8. New, J. H., Sugiyama, T., Zaitseva, E., and Kowalczykowski, S. C. (1998) *Nature* **391,** 407–410
9. Shinohara, A., Shinohara, M., Ohta, T., Matsuda, S., and Ogawa, T. (1998) *Genes Cells* **3,** 145–156
10. Sugiyama, T., New, J. H., and Kowalczykowski, S. C. (1998) *Proc. Natl. Acad. Sci. U. S. A.* **95,** 6049–6054
11. Wold, M. S. (1997) *Annu. Rev. Biochem.* **66,** 61–91
12. Van Dyck, E., Hajibagheri, N. M. A., Stasiak, A., and West, S. C. (1998) *J. Mol. Biol.* **284,** 1027–1038
13. Golub, E. I., Gupta, R. C., Haaf, T., Wold, M. S., and Radding, C. M. (1998) *Nucleic Acids Res.* **26,** 5388–5393
14. Baumann, P., and West, S. C. (1999) *J. Mol. Biol.* **291,** 363–374
15. Shen, Z., Cloud, K. G., Chen, D. J., and Park, M. S. (1996) *J. Biol. Chem.* **271,** 148–152
16. Park, M. S., Ludwig, D. L., Stigger, E., and Lee, S. H. (1996) *J. Biol. Chem.* **271,** 18996–19000
17. Benson, F. E., Baumann, P., and West, S. C. (1998) *Nature* **391,** 401–404
18. Shen, Z., Peterson, S. R., Comeaux, J. C., Zastrow, D., Moyzis, R. K., Bradbury, E. M., and Chen, D. J. (1996) *Mutat. Res.* **364,** 81–89
19. Kito, K., Wada, H., Yeh, E. T., and Kamitani, T. (1999) *Biochim. Biophys. Acta* **1489,** 303–314
20. Van Dyck, E., Stasiak, A. Z., Stasiak, A., and West, S. C. (1999) *Nature* **398,** 728–731
21. Stasiak, A. Z., Larquet, E., Stasiak, A., Muller, S., Engel, A., Dyck, E. V., West, S. C., and Egelman, E. H. (2000) *Curr. Biol.* **10,** 337–340
22. Henricksen, L. A., Umbricht, C. B., and Wold, M. S. (1994) *J. Biol. Chem.* **269,** 11121–11132
23. Wall, J. S., Hainfeld, J. F., and Simon, M. N. (1998) *Methods Cell Biol.* **53,** 139–164
24. Mortensen, U. H., Bendixen, C., Sunjevaric, I., and Rothstein, R. (1996) *Proc. Natl. Acad. Sci. U. S. A.* **93,** 10729–10734

Human RAD52 Protein Has Extreme Thermal Stability

Wasantha Ranatunga, Doba Jackson, Robert A. Flowers II, and Gloria E. O. Borgstahl

Department of Chemistry, The University of Toledo,
Toledo, Ohio 43606-3390

Biochemistry®

Human RAD52 Protein Has Extreme Thermal Stability[†]

Wasantha Ranatunga, Doba Jackson, Robert A. Flowers II, and Gloria E. O. Borgstahl*

Department of Chemistry, The University of Toledo, Toledo, Ohio 43606-3390

Received February 2, 2001; Revised Manuscript Received April 27, 2001

ABSTRACT: The human RAD52 protein plays an important role in the earliest stages of chromosomal double-strand break repair via the homologous recombination pathway. Individual subunits of RAD52 associate into seven-membered rings. These rings can form higher order complexes. RAD52 binds to DNA breaks, and recent studies suggest that the higher order self-association of the rings promotes DNA end joining. Monomers of the RAD52(1−192) deletion mutant also associate into ring structures but do not form higher order complexes. The thermal stability of wild-type and mutant RAD52 was studied by differential scanning calorimetry. Three thermal transitions (labeled A, B, and C) were observed with melting temperatures of 38.8, 73.1, and 115.2 °C. The RAD52(1−192) mutant had only two thermal transitions at 47.6 and 100.9 °C (labeled B and C). Transitions were labeled such that transition C corresponds to complete unfolding of the protein. The effect of temperature and protein concentration on RAD52 self-association was analyzed by dynamic light scattering. From these data a four-state hypothetical model was developed to explain the thermal denaturation profile of wild-type RAD52. The three thermal transitions in this model were assigned as follows. Transition A was attributed to the disruption of higher order assemblies of RAD52 rings, transition B to the disruption of rings to individual subunits, and transition C to complete unfolding. The ring-shaped quaternary structure of RAD52 and the formation of higher ordered complexes of rings appear to contribute to the extreme stability of RAD52. Higher ordered complexes of rings are stable at physiological temperatures in vitro.

RAD52[1] protein plays a critical role in mitotic and meiotic recombination as well as double-strand break repair (*1, 2*). On the basis of a series of protein−protein interaction assays and DNA binding studies (*3−5*), a domain map of human RAD52 (RAD52) was proposed by Park et al. (Figure 1). Electron microscopy (EM) studies of *Saccharomyces cerevisiae* and human RAD52 have revealed formation of ring-shaped structures (9−13 nm in diameter), as well as higher order aggregates (*6−8*). The RAD52 rings appear to be composed of seven subunits (*9*). EM studies also showed that RAD52 recognizes and binds to double-stranded DNA ends as an aggregated complex that ranges in size from approximately 15 to 60 nm in diameter (*8*). This binding promoted end-to-end association between DNA molecules and stimulated the ligation of both cohesive and blunt DNA ends (*8*). Recently, by studying wild type and two deletion mutants of RAD52 (Figure 1), we demonstrated that the self-association domain in the N-terminal half of RAD52 is responsible for ring formation and that elements in the C-terminal half of the molecule participate in the formation of higher order complexes of rings (*10*).

Due to the biological interest of human RAD52 and the apparent biochemical importance of RAD52 self-association in DNA repair, we studied its multiple levels of self-association and stability using biophysical methods. The stability of wild-type RAD52 was studied by differential scanning calorimetry (DSC). To investigate the basis for the extreme stability of RAD52 that was discovered, two mutants were also studied, RAD52(1−192) and RAD52(218−418) (Figure 1). The effects of temperature and protein concentration on the hydrodynamic radius (R_H) of RAD52 were studied by dynamic light scattering (DLS). Finally, a hypothetical model of the effects of protein aggregation state on thermal stability was developed.

MATERIALS AND METHODS

Protein Purification. The domain structures for wild-type RAD52, RAD52(1−192), and RAD52(218−418) are described in Figure 1. Proteins were expressed, purified under reducing conditions, and concentrated as described (*10*). Unfortunately, enterokinase cleavage was nonspecific, and the histidine-patch thioredoxin (Invitrogen) could not be separated from the 218−418 peptide (Jackson, unpublished results). After the extreme thermal stability of wild-type RAD52 was observed, subsequent purifications included a heat treatment step. The lysate was heated to 55 °C for 30 min prior to the chromatography steps. Samples were concentrated using an Ultrafree-15 centrifugal filter device. After each step of concentration, the samples were analyzed by DLS. Protein concentrations were determined using the Bradford assay (Bio-Rad) with bovine serum albumin as a standard.
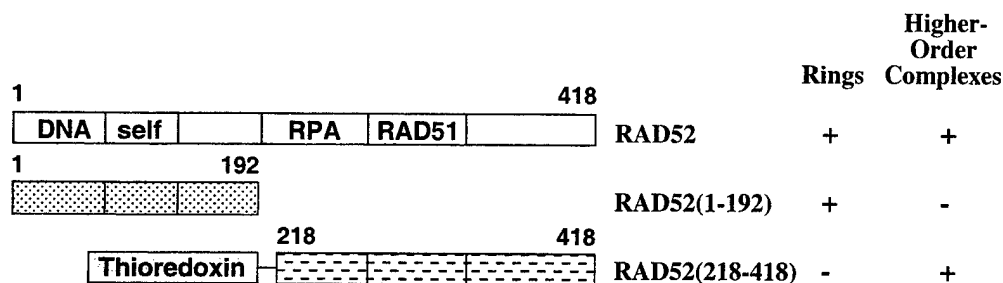
FIGURE 1: Wild-type RAD52 and deletion mutants. Beginning and ending residue numbers of each mutant are indicated along with domain structure. The following domains and residue numbers were defined by Park et al. (*16*): DNA binding (39−80), self-association (85−159), RPA binding (221−280), and RAD51 binding (290−330). The structural characterization of wild-type and mutant RAD52 by Ranatunga et al. is summarized on the right (*10*). Wild-type RAD52 and RAD51(1−192) have six histidines fused to the C-terminus. For the RAD52-(218−418) mutant, a thrombin-cleavable six-histidine tag is fused to the N-terminus of the histidine-patch thioredoxin, and an enterokinase cleavage site separates histidine-patch thioredoxin from RAD52(218−418).

Differential Scanning Calorimetry. Protein and reference solutions were degassed under a vacuum for 15 min before data acquisition. The concentration of wild-type RAD52 was 2.0 and 3.5 mg/mL, RAD52(1−192) was 7.2 mg/mL, and RAD52(218−418) was 3.1 mg/mL. The wild-type RAD52 sample was concentrated to 11.5 mg/mL before dilution to either 2.0 or 3.5 mg/mL. The concentrations of wild-type RAD52 and RAD52(218−418) were limited by the quantity of protein available. The protein samples and reference solutions were loaded into their respective cells in the MicroCal MC-2 differential scanning calorimeter. An external pressure of 30 psi was applied with nitrogen gas to both sample and reference cells. The sample was scanned relative to the reference solution over a temperature range of 5−120 °C at a rate of 45 °C/h. DSC measurements on buffer alone had no transitions for the temperature range 5−120 °C. The baseline and change in specific heat (ΔC_p) upon denaturation were corrected according to standard techniques (*11*). DSC data were fit to a two- or three-state model using the Origin DSC software provided by Microcal Inc.

Dynamic Light Scattering Analysis. DLS was carried out using a DynaPro-801 molecular sizing instrument equipped with a temperature-controlled microsampler (Protein Solutions). A 50 μL sample was passed through a filtering assembly equipped with a 100 nm filter into a 12 μL chamber quartz cuvette. For each experiment, 35−60 measurements were taken. The data were first analyzed using Dynamics 4.0 software and then with DynaLS software. The refractive index and viscosity of the buffer at each temperature were measured and the proper corrections applied to the data. Baseline and sum of squares (SOS) error values were reported by Dynamics 4.0. The baseline is the measured value of the last coefficient in the correlation curve. Baselines within the range from 0.977 to 1.002 were interpreted as monomodal, and those greater than 1.002 were bi- or multimodal. The SOS error is the sum of squares difference between the measured correlation curve and the best-fit curve. SOS errors less than 5.000 were considered negligible. Errors between 5.000 and 20.000 were considered as low and probably due to low protein concentration or a small amount of polydispersity. Errors greater than 20.000 were considered as high and are probably due to high polydispersity in size distribution (aggregation) or irregular solvent. Mean R_H, standard deviation, and percent of peak area are reported from DynaLS using the optimized resolution. Due to the irregular solvent, the SOS errors increased for diluted

samples, and it was necessary to use DynaLS to separate the solvent peak from the protein peak.

RESULTS AND DISCUSSION

Differential Scanning Calorimetry. Thermal stability profiles of wild-type RAD52, RAD52(1−192), and RAD52-(218−418) were obtained by DSC (Figure 2 and Table 1). For wild-type RAD52 and RAD52(1−192) the DSC transitions were labeled A, B, or C such that total unfolding was always labeled C. For wild-type RAD52, at 2.0 mg/mL, the DSC profile was composed of two transitions (labeled B and C) with melting temperatures (T_M) of 78.3 and 101.6 °C (Table 1). At 3.5 mg/mL, the wild-type RAD52 DSC profile was composed of three distinct transitions (labeled A, B, and C in Figure 2A) with T_M's of 38.8, 73.1, and 115.2 °C (Table 1). When the concentration of wild-type RAD52 was increased, transition C was shifted to a higher temperature by 13 °C. Transition A could be measured only if the sample was first concentrated to 11.5 mg/mL and then diluted to 3.5 mg/mL. For RAD52(1−192) two transitions were observed at 47.6 and 100.9 °C (labeled B and C in Figure 2B). The deletion of the C-terminal half of RAD52 decreased the T_M of transitions B and C by 25 and 14 °C, respectively.

Our earlier analysis demonstrated that wild-type RAD52 forms ring structures as well as higher order complexes of rings but RAD52(1−192) forms rings but not the aggregates of rings (*10*). The size of the wild-type RAD52 higher order complexes, as well as the proportion of the rings in a higher order complex, is dependent on concentration. RAD52(1−192) rings do not form higher ordered complexes, at any concentration. DSC transition A was dependent on the concentration of wild-type RAD52 and was not observed for RAD52(1−192). Therefore, it appeared that transition A corresponded to the thermal disruption of aggregates to form single rings in solution, transition B to the break up of rings to monomers, and transition C to the total unfolding of monomers.

The DSC profile of RAD52(218−418) is also consistent with this interpretation (Figure 2C). RAD52(218−418) forms a complex of two to four monomers depending on the concentration but does not form ring structures in solution (*10*). It has a relatively low T_M of 53−59 °C, and it appears that the C-terminal half of RAD52, which cannot form rings, is not as thermally stable as the ring-structured N-terminal half.

Wild-type *Escherichia coli* thioredoxin is a very stable protein with a T_M of ~85 °C for the oxidized form and ~73

Table 1: Thermodynamic Parameters from DSC Measurement of RAD52 Proteins

protein	concn (mg/mL)	component	T_M (°C)
RAD52[a]	2.0	B	78.3
		C	101.6
RAD52[b]	3.5	A	38.8
		B	73.1
		C	115.2
RAD52(1−192)[c]	7.2	B	47.6
		C	100.9
RAD52(218−418)[d]	3.1	1	53.4
		2	59.1

[a] This sample was concentrated to 11.5 mg/mL and then diluted to 2.0 mg/mL (similar to Table 2, line 12) and does not contain higher ordered assemblies of rings. [b] This sample was concentrated to 11.5 mg/mL and then diluted to 3.5 mg/mL for DSC measurements (similar to Table 2, line 7, and Figure 3E) and contains higher ordered complexes of rings. [c] RAD52(1−192) forms rings but does not form higher ordered assemblies of rings (10). [d] RAD52(218−418) does not form rings but does self-associate (10).

ably have a T_M lower than that measured for the fusion protein.

The reversibility of transitions A, B, and C for wild-type RAD52 was studied by DSC, using an 11.5 mg/mL sample diluted to 3.5 mg/mL. Three experiments were performed, and the presence of precipitation was noted after each (data not shown). First, the sample was heated to 55 °C and then slowly returned to 20 °C overnight. Transition A was observed, and the protein remained in solution. Then the same sample was heated to 95 °C and slowly returned to 20 °C overnight. During this second experiment, transition A did not return, possibly due to the protein concentration used (see discussion of DLS data, Table 2, lines 7−9), and transition B was lowered to 65 °C. After the second experiment there was a slight amount of precipitate, but the majority of the protein was still in solution. For the third experiment, the sample was heated to 120 °C, and there was only one significant peak at 94 °C and the protein completely precipitated. The T_M for complete unfolding was lower than that measured from fresh sample (115 °C for peak C, Figure 2A), indicating that the protein did not properly reassemble after the second experiment and that the process of unfolding is irreversible under this set of experimental conditions.

The irreversibility of transition B was also noted in experiments performed during the addition of a heat step to the purification protocol for wild-type RAD52. Lysates were heated in 5 deg increments between 55 and 80 °C, centrifuged, and analyzed by SDS−PAGE. RAD52 began to precipitate after 65 °C (data not shown). This supports the conclusion that transition B in the thermal denaturation of RAD52 is irreversible.

Dynamic Light Scattering. The response of RAD52 rings and higher ordered complexes to concentration and temperature was studied by DLS. The upper temperature limit of the DLS microsampler was 50 °C so theoretically data on transition A of wild-type RAD52 and transition B of RAD52-(1−192) could be measured.

The procedure followed for sample preparation affected the detection of DSC transition A and the T_M value of transition C for wild-type RAD52, so the effects of protein concentration and temperature on the R_H of wild-type RAD52 were studied using DLS. In a series of experiments, the protein concentration was increased from 3.5 to 11.5 mg/
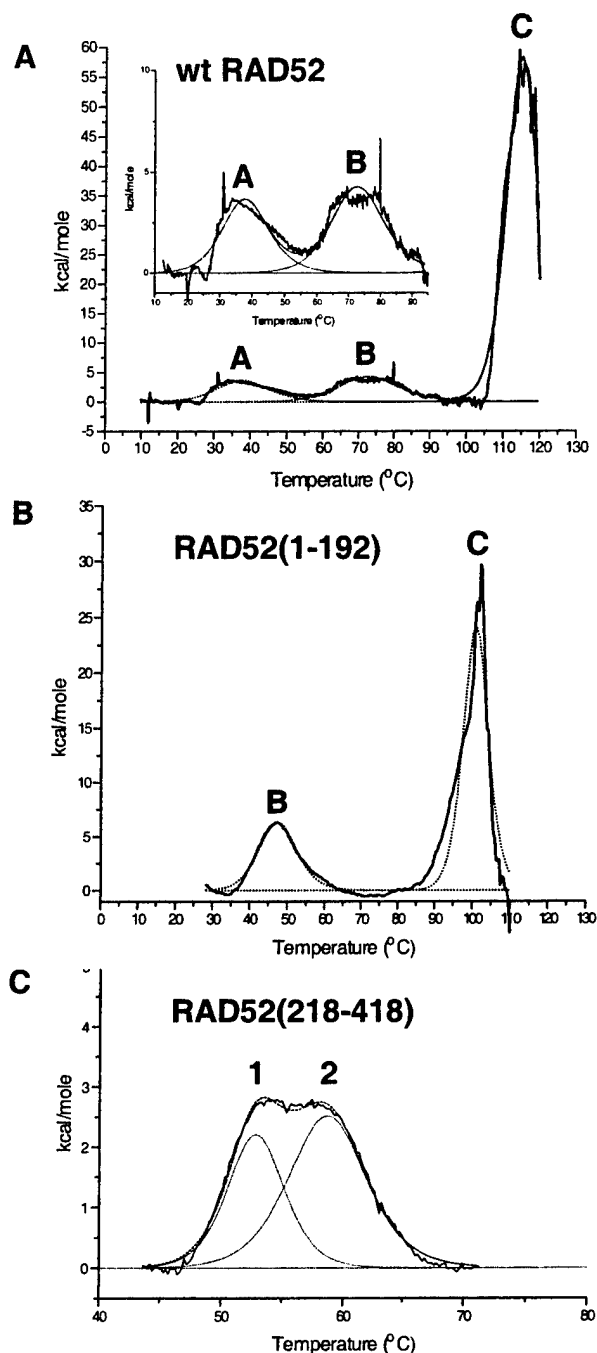
Figure 2: Thermal stability of wild-type RAD52 and deletion mutants. DSC profiles for (A) wild-type RAD52 were analyzed at 0.038 mM (3.5 mg/mL), (B) RAD52(1−192) at 0.325 mM (7.2 mg/mL), and (C) RAD52(218−418) at 0.082 mM (3.1 mg/mL). For RAD52(218−418) there were no transitions above 70 °C.

°C for the reduced form (12, 13). When thioredoxin is fused to other proteins, it can improve their solubility and, especially when in the oxidized form, improve their thermal stability, allowing a heat step during purification. Histidine-patch thioredoxin in the reduced state was expected to have a T_M of ∼67 °C (12−14). We were unable to specifically cleave thioredoxin from RAD52(218−418) with enterokinase, so the exact contributions of thioredoxin and RAD52-(218−418) to the DSC profile of the fusion protein could not be determined. It is apparent that fusing thioredoxin to RAD52(218−418) has reduced the T_M of thioredoxin significantly and that RAD52(218−418) by itself would prob-

Table 2: Effect of Temperature and Concentration on R_H of Wild-Type RAD52

DLS expt	concn (mg/mL)	base-line	SOS error[a]	$R_H{}^b$ (nm)	peak area[c] (%)	interpre-tation[d]
1. 20 °C	3.5	1.001	4.22	**15.0 (2.5)**	**98.3**	>2 rings
2. heat to 50 °C	3.5	1.000	2.78	**14.2 (4.5)**	**99.2**	~2 rings
3. concd; 20 °C	4.9	1.002	2.03	4.3 (0.5)	3.4	monomer
				18.7 (2.3)	**95.8**	>2 rings
4. concd; 20 °C	11.5	1.009	7.78	5.1 (0.6)	4.2	mono/dimer
				17.8 (3.1)	**56.9**	>2 rings
				36.1 (4.4)	**36.6**	≫2 rings
5. heat to 50 °C	11.5	1.000	5.96	**19.2 (8.5)**	**99.2**	>2 rings
6. cool to 20 °C	11.5	1.010	8.24	5.9 (0.4)	9.7	mono/dimer
				11.2 (0.7)	6.6	1−2 rings
				20.6 (2.2)	**81.6**	>2 rings
7. sample from line 4 diluted; 20 °C	3.5	1.001	11.3	3.8 (0.2)	0.6	monomer
				23.2 (11.6)	**98.1**	>2 rings
8. heat to 50 °C	3.5	1.001	9.41	**9.7 (1.2)**	**45.8**	1 ring
				17.0 (1.0)	**49.8**	>2 rings
9. cool to 20 °C	3.5	1.001	16.1	3.9 (0.2)	1.1	monomer
				11.9 (1.9)	**69.3**	1−2 rings
				28.6 (3.5)	**26.4**	≫2 rings
10. sample from line 3 diluted; 20 °C	3.3	1.001	7.4	**3.1 (0.2)**	**11.0**	monomer
				16.8 (5.4)	**84.0**	>2 rings
				49.5 (8.7)	**14.5**	≫2 rings
11. heat to 37 °C	3.3	1.000	7.9	**19.8 (10.9)**	**99.5**	>2 rings
12. sample from line 4 diluted; 20 °C	2.3	1.001	50.9	**8.75 (6.0)**	**79.7**	1 ring
13. heat to 37 °C	2.3	1.000	24.5	**8.0 (1.6)**	**71.9**	1 ring
14. heat to 50 °C	2.3	1.000	15.9	**8.7 (2.7)**	**87.4**	1 ring

[a] SOS = sum of squares. [b] Average R_H is given with the standard deviation given in parentheses. [c] DynaLS results; the percent peak area for the solvent peaks was not reported. DLS measurements at 20 and 50 °C on solvent alone indicate that very small and very large components in the RAD52 measurements were due to the solvent and not the protein. Therefore, only the peaks attributable to RAD52 protein are reported (R_H > 3.0 nm; see Figure 4). R_H and percent peak area of the primary species in solution (greater than 10%) are in bold. [d] Interpretation is based on estimated R_H in Figure 4. It is not possible to tell exactly how many rings of RAD52 are in the aggregates >14.1 nm since the structure of the higher order complexes of RAD52 rings is unknown.

mL and then diluted (see Table 2 and Figure 3). The microsampler cell was held at 20, 37, or 50 °C, and samples were equilibrated for 30 min at the target temperature before DLS measurements began. The smallest R_H measured for RAD52 was 8.0−8.75 nm (Table 2, lines 12−14). This is close to the size expected for single rings measured from electron micrographs (Figure 4) (6−8). A monomer of RAD52 is expected to have an R_H value of 3.2 nm, and complexes containing two rings are expected to have an R_H of 12.8−14.1 nm. The R_H for aggregates of more than two rings would be greater than 14 nm.

Using these estimates of particle sizes as a guide, four trends in the DLS data were noted. First, heating the protein samples from 20 to 50 °C caused the R_H to decrease in general, and frequently the baseline decreased to within the monomodal range. For example, heating a sample similar to that used for DSC measurements (Table 2, line 7, and Figure 3E) caused the particles to shift from a single population with R_H of 23.2 nm to two populations with R_H of 9.7 and 17.0 nm (Table 2, line 8, and Figure 3F). Second, the size of the sample population was dependent on the protein concentration. For example, the R_H of the sample
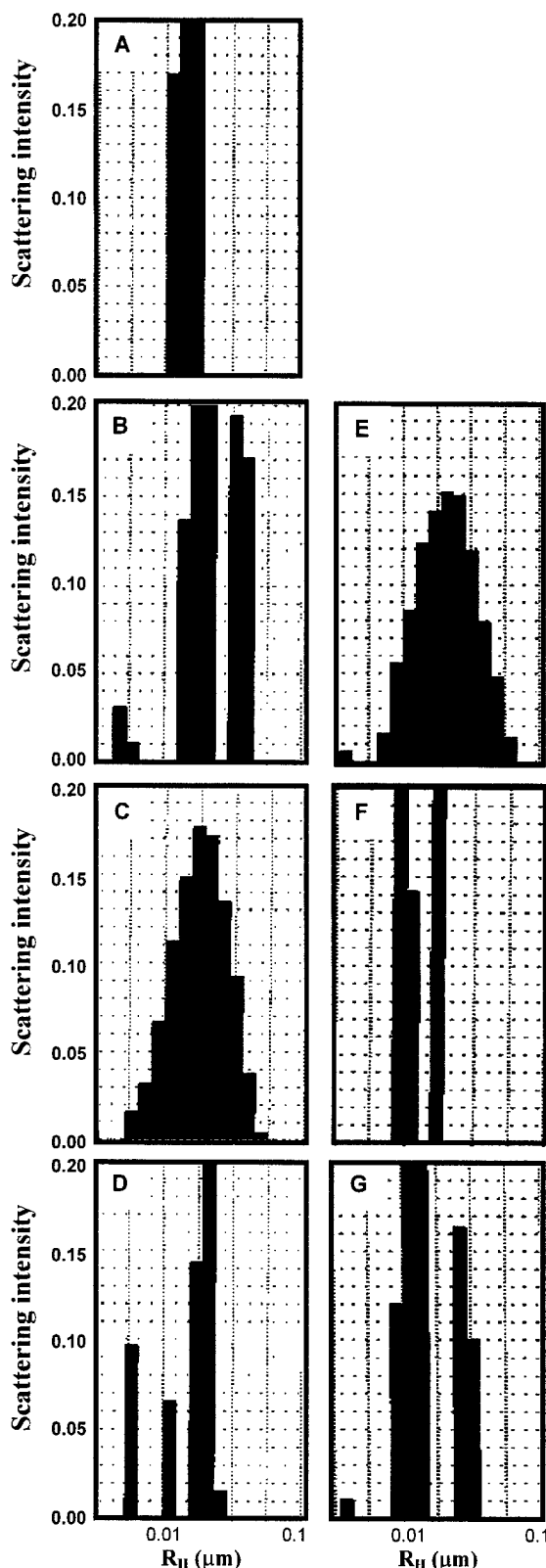

FIGURE 3: Effect of protein concentration and temperature on the R_H of wild-type RAD52. DLS data were analyzed using DynaLS software. The data correspond to the following lines in Table 2: (A) 3.5 mg/mL at 20 °C (line 1), (B) 11.5 mg/mL at 20 °C (line 4), (C) 11.5 mg/mL at 50 °C (line 5), (D) 11.5 mg/mL cooled to 20 °C (line 6), (E) diluted to 3.5 mg/mL at 20 °C (line 7), (F) diluted to 3.5 mg/mL at 50 °C (line 8), and (G) diluted to 3.5 mg/mL cooled to 20 °C (line 9). Panels E−G correspond to the sample used for DSC.
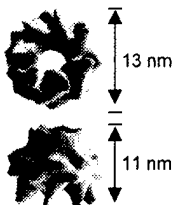
Model	R_H (nm)
Monomer	3.2
7-membered ring	8.5
Two edge on rings	14.1
Two stacked rings	12.8

13 nm

11 nm

FIGURE 4: Estimated R_H for RAD52 models. The R_H for a monomer was calculated from a molecular mass of 47.0 kDa with the molecular weight calculator included in the Dynamics 3.0 software. R_H for a seven-membered ring of RAD52 was estimated from the diagonal of the three-dimensional reconstruction on the basis of electron micrographs (9). Electron micrographs of RAD52 rings in the large, greater than 100 nm spherical aggregates appear to have an "edge-on" orientation (10). The three-dimensional reconstructions of RAD52 were adapted from Stasiak et al. (2000).

population increased from 15.0 to 18.7 to 36.1 nm, when the concentration was increased from 3.5 to 4.9 to 11.5 mg/mL (Table 2, lines 1, 3, and 4). Third, the modality of the sample population was dependent on the protein concentration. For example, the 11.5 mg/mL sample was multimodal at 20 °C (Table 2, line 4, and Figure 3B), and the 3.5 mg/mL sample was not (Table 2, line 1, and Figure 3A). Fourth, the reversibility of the assembly of RAD52 rings into higher ordered complexes was dependent on protein concentration. The majority of the particles in the samples at 11.5 mg/mL remained greater than 17 nm throughout the heat cycle (Table 2, lines 4–6, and Figure 3B–D). But, the superaggregation of rings was only partially reversible at 3.5 mg/mL with only 26% of the sample returning to greater than 17 nm after being heated (Table 2, lines 7–9, and Figure 3E–G). It is noteworthy that for the DSC measurements made on samples at 3.5 mg/mL the assembly of RAD52 rings into higher ordered complexes is not completely reversible at this concentration.

Finally, this DLS analysis facilitated the interpretation of DSC transition A. Transition A could not be detected for samples that were first concentrated to 11.5 mg/mL and then diluted to 2.0 mg/mL (prepared as in line 12, Table 2). The R_H value of 8.75 indicates that at 2.0 mg/mL there are primarily single rings in solution and little or no higher ordered complexes (Figure 4). Transition A was detectable for samples that were diluted to 3.5 mg/mL (prepared as in line 7, Table 2, and Figure 3E). The R_H value of 23.2 nm indicates that at 3.5 mg/mL there are primarily higher order complexes of many rings in solution. Heating this sample to 50 °C caused the R_H to decrease and form two populations of 9.7–17.0 nm (Table 2, line 8, and Figure 3F). Therefore, these DLS data indicate that DSC transition A can be attributed to the disassociation of rings from higher ordered complexes.

We were interested to know if the higher ordered complexes of RAD52 rings were stable at physiological temperatures. Protein samples diluted to 3.3 mg/mL did not form particles less than 9 nm upon heating to 37 °C (Table 2, lines 10 and 11) although the samples became monomodal. Therefore, the upper level aggregation of RAD52 rings is stable at physiological temperatures in vitro.

Transition B of the RAD52(1–192) mutant was 47.6 °C, and attempts were made to measure the effect of temperature on the structure of RAD52(1–192) with DLS. Higher ordered assemblies of rings are not formed by RAD52(1–
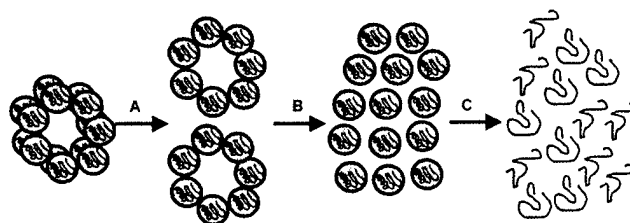

FIGURE 5: Hypothetical four- state model for the thermal denaturation of wild-type RAD52. Transitions A, B, and C correspond to those measured by DSC in Figure 2. There are three transitions in this model; transition A is attributed to the disruption of higher order assemblies of RAD52 rings, transition B to the disruption of rings to individual subunits, and transition C to complete unfolding. The individual subunits after transition B are probably partially unfolded as well as disassociated from the rings.

192), and single rings have an R_H of 5.7 nm (SD = 1.2) (10). As samples of RAD52(1–192) were heated, the R_H appeared to increase, perhaps indicating partial unfolding (data not shown). DLS measurements at elevated temperatures with RAD52(1–192) were very problematic, and at 50 °C no measurements could be obtained, perhaps due to large changes in structure.

CONCLUSIONS

Our data indicate that the RAD52 rings and higher ordered complexes of rings used in DNA repair and DNA recombination are extremely stable structures. The structure of wild-type RAD52 is very stable, and its multiple levels of self-association appear to contribute to this stabilization. The extreme stability of the wild-type RAD52 and RAD52(1–192) folds relative to RAD52(218–418) appears to be related to the assembly of multiple monomers into a ring. The enhanced stability of the wild-type RAD52 fold relative to RAD52(1–192) appears to be due in part to its ability to form higher order assemblies of rings.

A four-state hypothetical model has been developed to explain the thermal denaturation profile of wild-type RAD52 (Figure 5). There are three transitions in this model; transition A is attributed to the disruption of higher order assemblies of RAD52 rings, transition B to the disruption of rings to individual subunits, and transition C to complete unfolding. Individual rings of RAD52 appear to have an R_H on the order of 8.0–8.75 nm in solution (Table 2, lines 12–14). Higher order assemblies of rings are seen in the wild-type RAD52 DLS data as particles ranging from 15 to 50 nm. Note that the measured R_H values are not integral values of individual rings due to the presence of equilibrium mixtures of single rings and complexes of rings in solution as indicated by the high standard deviations in the R_H measurements (Table 2) and the width of the DLS peaks (Figure 3). This equilibrium is dependent upon concentration. At concentrations of 3.5 mg/mL or greater RAD52 appears to be primarily composed of assemblies of two or more rings with R_H values ranging from 15 to 36.1 nm. Raising the temperature from 20 to 50 °C disrupts the higher order particles, pushing the equilibrium toward the 9 nm particles (Table 2, lines 5 and 8, and Figure 3C and F). These data support our hypothetical model for transition A (Figure 5). Reliable DLS measurements varying temperature on RAD52(1–192) could not be made. Thermal expansion of the RAD52(1–192) rings was noted. The data indicate that a large structural transition occurs near transition

B, possibly the disassociation of individual subunits from the rings.

Only a handful of proteins have been measured with thermal stabilities on the order of RAD52. To our knowledge, the highest T_M for a protein reported in the literature to date is 125 °C for ferredoxin from the hyperthermophile *Thermotoga maritima* (*15*). Other proteins such as onconase and mitochondrial manganese superoxide dismutase (MnSOD) are extremely stable with T_M's approaching 90 °C (*16, 17*). Both ferredoxin and onconase are monomeric, and by studying their protein crystal structures, their stabilities were attributed to the compactness of their tertiary structures and to extensive hydrogen bonding involving charged amino acid side chains. Mitochondrial MnSOD is a homotetramer, and its enhanced stability was partially attributed to its quaternary structure. The DSC profile of MnSOD has three thermal transitions (labeled A, B, and C), similar to those seen with RAD52. Transition A was attributed to subunit disassociation, transition B to loss of the active site manganese, and transition C to complete unfolding. A cavity forming point mutation in the tetrameric interface of MnSOD resulted in the lowering of transition B by 13.6 °C and transition C by 16.5 °C (*17*). These results on MnSOD are somewhat similar to the results on RAD52. We conclude from our data that both components of RAD52 self-association, ring formation and higher order complex formation, contribute to its extreme thermal stability. A precise understanding of the structural determinants of RAD52 stability awaits the solution of its crystal structure.

ACKNOWLEDGMENT

REFERENCES

1. Game, J., and Mortimer, R. K. (1974) *Mutat. Res. 24*, 281−292.
2. Petes, T. D., Malone, R. E., and Symington, L. S. (1991) in *The Molecular and Cellular Biology of the Yeast, Saccharomyces* (Broach, J. R., Pringle, J. R., and Jones, E. W., Eds.) pp 407−522, Cold Spring Harbor Laboratory Press, Cold Spring Harbor, NY.
3. Shen, Z., Cloud, K. G., Chen, D. J., and Park, M. S. (1996) *J. Biol. Chem. 271*, 148−152.
4. Shen, Z., Peterson, S. R., Comeaux, J. C., Zastrow, D., Moyzis, R. K., Bradbury, E. M., and Chen, D. J. (1996) *Mutat. Res. 364*, 81−89.
5. Park, M. S., Ludwig, D. L., Stigger, E., and Lee, S. H. (1996) *J. Biol. Chem. 271*, 18996−19000.
6. Shinohara, A., Shinohara, M., Ohta, T., Matsuda, S., and Ogawa, T. (1998) *Genes Cells 3*, 145−156.
7. Van Dyck, E., Hajibagheri, N. M. A., Stasiak, A., and West, S. C. (1998) *J. Mol. Biol. 284*, 1027−1038.
8. Van Dyck, E., Stasiak, A. Z., Stasiak, A., and West, S. C. (1999) *Nature 398*, 728−731.
9. Stasiak, A. Z., Larquet, E., Stasiak, A., Muller, S., Engel, A., Dyck, E. V., West, S. C., and Egelman, E. H. (2000) *Curr. Biol. 10*, 337−340.
10. Ranatunga, W., Jackson, D., Lloyd, J. A., Forget, A. L., Knight, K. L., and Borgstahl, G. E. O. (2001) *J. Biol. Chem.* (in press).
11. Haynie, D. T., and Freire, E. (1994) *Anal. Biochem. 216*, 33−41.
12. Ladbury, J., Wynn, R., Hellinga, H., and Sturtevant, J. (1993) *Biochemistry 32*, 7526−7530.
13. Ladbury, J., Kishore, N., Hellinga, H., Wynn, R., and Sturtevant, J. (1994) *Biochemistry 33*, 3688−3692.
14. Lu, Z., DiBlasio-Smith, E., Grant, K., Warne, N., LaVallie, E., Collins-Racie, L., Follettie, M., Williamson, M., and McCoy, J. (1996) *J. Biol. Chem. 271*, 5059−5065.
15. Pfeil, W., Gesierich, U., Kleemann, G. R., and Sterner, R. (1997) *J. Mol. Biol. 272*, 591−596.
16. Notomista, E., Catanzano, F., Graziano, G., Piaz, F. D., Barone, G., D'Alessio, G., and Donato, A. D. (2000) *Biochemistry 39*, 8711−8718.
17. Borgstahl, G. E. O., Parge, H. E., Hickey, M. J., Johnson, M. J., Boissinot, M., Hallewell, R. A., Lepock, J. R., Cabelli, D. E., and Tainer, J. A. (1996) *Biochemistry 35*, 4287−4297.

Human Rad52 protein has extreme thermal stability

Wasantha Ranatunga
Research Advisor: Dr. Gloria Borgstahl
Department of Chemistry
Phone: (419) 530 1581
Email: wranatunga@hotmail.com

Human Rad52 (hRAD52) is double-strand break repair protein involved in the homologous recombination pathway (1). The monomers of hRAD52 self-associate into rings as well as higher order aggregates of rings (2). hRAD52 binds to DNA double-strand ends and mediates strand exchange or end joining by higher order association (3). The thermal stability of hRAD52 was investigated using differential scanning calorimetry. In the profile of calorimetry, three transitions were observed at temperatures of 38.8, 73.1 and 115.2 °C. The two-domain mutant, hRAD52 (1-192) showed two transitions at 47.6 and 100.9 °C and does not form higher order aggregates of rings. Dynamic light scattering (DLS) was used to study structural changes of hRAD52 due to concentration and temperature. Data indicate an increase in aggregation with concentration. The aggregates of rings can be disrupted at higher temperatures. Aggregation of rings, as well as ring formation, appear to stabilize the fold and a four state hypothetical model was proposed to explain the thermal denaturation profile of wild-type hRAD52.

1. Shinohara, A., Shinohara, M., Ohta, T., Matsuda, S., and Ogawa, T. *Genes to Cells* **3**, 145, (1998).
2. Van Dyck, E., Hajibagheri, N. M. A., Stasiak, A., and West, S. C. *J. Mol. Biol.* **284**, 1027, (1998).
3. Van Dyck, E., Stasiak, A., and West, S. C. *Nature* **398**, 728, (1999).

Wasantha Ranatunga, Doba Jackson, R. A. Flowers II and Gloria E. O. Borgstahl, Human RAD52 has extreme thermal stability. First annual biomolecular sciences day (March 24, 2001)

Abstract:

The human Rad52 (hRAD52) protein plays an important role in the earliest stages of chromosomal double-strand break repair via the homologous recombination pathway. Individual subunits of hRad52 self-associate into rings that can then form higher-order complexes. hRad52 binds to double-strand DNA ends and recent studies suggest that the higher order self-association of the rings promotes DNA end joining. The thermal stability of hRad52 was studied by differential scanning calorimetry. Three thermal transitions were observed with melting temperatures of 38.8, 73.1 and 115.2 °C. The hRad52(1-192) mutant that does not form higher ordered complexes of rings had only two thermal transitions at 47.6 and 100.9 °C. The effect of temperature and protein concentration on hRad52 structures was analyzed by dynamic light scattering. From these data a four state hypothetical model was proposed to explain the thermal denaturation profile of wild-type hRad52. The three thermal transitions in this model were assigned as follows. Transition A was attributed to the disruption of higher order assemblies of hRad52 rings, transition B to the disruption of rings to individual subunits and transition C to complete unfolding. The extreme stability of hRad52 was attributed to is ring-shaped quaternary structure and to the formation of higher ordered complexes of rings. Higher ordered complexes of rings appear to be stable at physiological temperatures *in vitro*.

BIOCHEMICAL AND STRUCTURAL STUDIES ON REPLICATION PROTEIN A AND RAD52

Gloria E. O. Borgstahl, Wasantha Ranatunga, Doba Jackson and Jeff Habel

Department of Chemistry, The University of Toledo, Toledo, OH 43606

E-mail: gborgst@uoft02.utoledo.edu

Replication Protein A (RPA) and RAD52 are both involved in the metabolism of DNA. RPA is composed of 70, 32 and 14 kDa subunits and has two forms, heterotrimeric and heterodimeric (RPA14/32). RPA heterotrimer is essential for the replication of DNA and is intrinsic to DNA transcription, recombination and repair. RPA14/32 separates from the heterotrimer during apotosis. RAD52 is a 50 kDa protein that forms ring structures composed of 8-10 subunits. RAD52 is fundamental to the recombination-based repair of double-strand DNA breaks. RPA, RAD52 together with RAD51 are responsible for the first steps of double-strand DNA break repair. Most interestingly, the breast cancer genes BRCA1 and BRCA2 have been associated with the double-strand DNA break repair pathway. Biochemical studies on the protein-protein interactions between RPA, RAD52 and RAD51 as well as the self-association of RAD52 will be presented. Protein crystallographic studies on RPA will be presented. We have crystallized the RPA14/32 dimer in three crystal forms. X-ray diffraction data to 2.0 Å resolution has been collected and the phase problem solved through molecular replacement. Up-to-date structural results will be presented. It is anticipated that the three-dimensional structure of the RPA32 C-terminal protein-protein interaction domain will be revealed in these studies.